

## **General Disclaimer**

### **One or more of the Following Statements may affect this Document**

- This document has been reproduced from the best copy furnished by the organizational source. It is being released in the interest of making available as much information as possible.
- This document may contain data, which exceeds the sheet parameters. It was furnished in this condition by the organizational source and is the best copy available.
- This document may contain tone-on-tone or color graphs, charts and/or pictures, which have been reproduced in black and white.
- This document is paginated as submitted by the original source.
- Portions of this document are not fully legible due to the historical nature of some of the material. However, it is the best reproduction available from the original submission.

# Generation of the Auroral Kilometric Radiation

✓ Prepared by

C. S. WU and H. K. WONG  
Institute for Physical Science and Technology  
University of Maryland  
College Park, Md. 20742

D. J. GORNEY  
Space Sciences Laboratory  
The Aerospace Corporation  
El Segundo, Calif. 90245

and

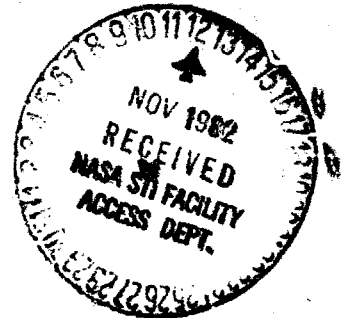
L. C. LEE  
Geophysical Institute  
University of Alaska  
Fairbanks, Alaska 99701

1 November 1982

Prepared for

NATIONAL SCIENCE FOUNDATION  
Washington, D.C. 20550

Contract No. ATM 8C00518



Programs Group

THE AEROSPACE CORPORATION

(NASA-CR-169532) GENERATION OF THE AURORAL  
KILOMETRIC RADIATION (Maryland Univ.) 53 p  
HL A04, MF A01 CSCL 04A

N83-13601

Unclass

G3/46 00778

GENERATION OF AURORAL  
KILOMETRIC RADIATION

C. S. Wu and H. K. Wong  
Institute for Physical Science and Technology  
University of Maryland  
College Park, Md. 99701

D. J. Gorney  
Space Sciences Laboratory  
THE AEROSPACE CORPORATION  
El Segundo, Calif. 90245

and

L. C. Lee  
Geophysical Institute  
University of Alaska  
Fairbanks, Alaska 99701

1 November 1982

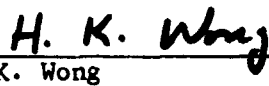
Prepared for  
NATIONAL SCIENCE FOUNDATION  
Washington, D.C. 20550

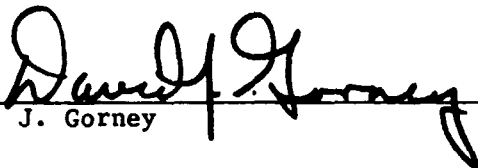
Contract No. ATM 8000518

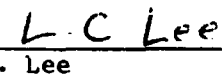
GENERATION OF AURORAL  
KILOMETRIC RADIATION

Prepared

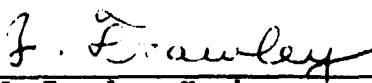
  
C. S. Wu

  
H. K. Wong

  
D. J. Gorney

  
L. C. Lee

Approved

  
J. Frawley, Head  
Mathematics and Analysis  
Department

  
H. R. Rugge, Director  
Space Sciences Laboratory

## ABSTRACT

In two preceding papers (Wu and Lee, 1979; Lee et al., 1980) an effective loss-cone distribution function is used in the stability analysis relevant to the theory of auroral kilometric radiation. Furthermore, in these discussions it is assumed that the population of low-energy background electrons prevails over that of the energetic electrons. Obviously, this assumption may not be justifiable at high altitude. The present work considers a loss-cone distribution close to that observed and, moreover, includes the effect of a parallel electric field along the auroral magnetic field lines. It is found that this effect tends to enhance the growth rate. We have also removed the assumption concerning the high population of background electrons. We find that at high altitudes, where the density of energetic electrons may dominate and the usual cold-electron dispersion relation is invalid, the cutoff frequency of the X mode can be significantly affected by the energetic electrons and thereby the growth rate is indirectly altered. In the present discussion, the emission of the auroral kilometric radiation is studied over a range of altitudes. We have considered three density models and two electric field models. Temporal growth rates and e-folding distances of spatial amplification are computed and discussed.

## ACKNOWLEDGMENTS

The present research was supported by the National Aeronautics and Space Administration under grant NGL 21-002-005 to the University of Maryland, by the U. S. Air Force Contract No. F0 4701-80-C-0081 and National Science Foundation Contract ATM 8000518 to the Aerospace Corporation, and by the National Science Foundation grant ATM 79-16470 to the University of Alaska. The numerical computation was supported by the Computer Science Center of the University of Maryland.

The material presented in this paper also constitutes a portion of the Ph. D. dissertation by H. K. W.

During the course of this work we have enjoyed several inspiring, fruitful, and enthusiastic discussions with Don Gurnett, whose pioneering AKR observations have greatly motivated our interest in the subject.

## CONTENTS

ABSTRACT.....	v
ACKNOWLEDGMENTS.....	vi
I. INTRODUCTION.....	1
II. PHYSICAL MODEL.....	5
A. Model Distribution Function Based on Spacecraft Observations....	5
B. Magnetic Field and Electron Density.....	9
C. Parallel Electric Field.....	11
III. DISPERSION EQUATION.....	19
A. Resonance Condition.....	20
B. Method of Calculating the Dielectric Tensor $\epsilon_{ij}$ .....	22
C. Expression for $Q_{ij}^{\epsilon}(n=1)$ .....	26
IV. RESULTS AND DISCUSSION.....	27
A. Numerical Method.....	27
B. Results of Computation.....	28
C. Discussion.....	35
REFERENCES.....	41
APPENDIX.....	45

## FIGURES

1.	S3-3 Particle-Wave Spectrogram from Day 237, 1976.....	6
2.	An Electron Velocity-Space Distribution Taken at 17473 Seconds UT on Day 237, 1976.....	8
3.	Plot Showing the Dependence of Electron Gyrofrequency and Loss Cone Angle in Altitude Along Auroral Field Lines.....	10
4a.	Plot Showing the Modeled Dependence of the Electron Plasma Frequency for the Altitude Range of Interest.....	13
4b.	Same as Figure 4a, but Showing the Dependence of the Ratio of the Squares of the Plasma Frequency to the Electron Gyro- Frequency.....	14
5.	Plot of the Two Potential Distribution Models Used in the Wave Growth Calculations.....	16
6.	Schematic Plot Showing the Shape of the Relativistic Resonant Surface for the Extraordinary Mode.....	21
7.	Normalized Growth Rate Versus Altitude for Density Models A, B, C and D, With and Without Parallel Electric Field.....	29
8.	Normalized Amplification Distance Versus Altitude for Models With and Without Parallel Electric Field.....	30
9.	Same as Figure 8, but Depicting Case C With a Parallel Electric Field.....	31
10.	Real and Imaginary Frequency Versus Wave Number for Wave Normal Angles of $\theta = 0^\circ, 30^\circ, 45^\circ$ and $60^\circ$ , Case A.....	32
11.	Same as Fig. 10, but for Case C.....	33
12.	Same as Fig. 10, but With No Parallel Electric Field.....	34
13.	Schematic Figure Depicting the Physics of the Amplification Process.....	36



**TABLES**

1.	Density and Magnetic Field Models.....	12
2.	Models of the Parallel Electric Field and Auroral-Electron Energies.....	17

## I. INTRODUCTION

In two preceding articles (Wu and Lee, 1979; Lee et al., 1980) a theory of the auroral kilometric radiation (AKR) is proposed. The basic physical notion is that only a fraction of the energetic (keV) electrons originated in the plasma sheet can precipitate in the auroral region because those with pitch angles greater than the atmospheric loss-cone angle are expected to be reflected by the convergent magnetic field before they can reach the upper atmosphere. These reflected electrons are expected to possess a loss-cone distribution function which can result in the amplification of electromagnetic waves with frequency very near the electron gyro-frequency when the electron plasma frequency is sufficiently lower than the gyro-frequency (Wu and Lee, 1979). The emission mechanism is basically a cyclotron maser process.

In addition to the hypothesis that the upgoing keV electrons can possess a loss-cone distribution, Wu and Lee (1979) also suggested that the parallel electric field of inverted-V events (Gurnett, 1972; Mizera and Fennell, 1977; Croley et al., 1978; Mozer et al., 1977; Wescott et al., 1976) can deplete the low-energy electrons of ionospheric origin in the auroral flux tube, thereby reducing the local value of the electron plasma frequency. This process can increase the growth rate of the instability and, moreover, result in temporary wave trapping inside the source region. Evidently both consequences are important to the emission process of AKR.

Since the publication of the first article by Wu and Lee (1979), we have been encouraged by the facts that the S3-3 observations confirm our loss-cone hypothesis (private communications with Mizera, Fennell and Croley) and the ISIS-1 results clearly show that the predicted density depletion in the AKR source region is real (Benson and Calvert, 1979; Benson, Calvert and Klumpar, 1980; Calvert, 1981). Furthermore,

observations by Hawkeye (Gurnett and Green, 1978), by Voyager 1 (Kaiser et al., 1978) and by ISIS-1 (Benson and Calvert, 1979) all seem to indicate that the polarization of AKR is in the fast extraordinary mode (or X mode), which is consistent with our theory. Our analysis shows that although the amplification of the ordinary mode (or O mode) is possible, the process is much less effective than that for the X mode. Of course, it should be mentioned that the X mode polarization has also been predicted by other theories (Malrose, 1976; Grabbe, 1980). Physically it can be easily understood from linearized Vlasov theory why the growth rate associated with the X mode is larger than that of the O mode. Furthermore, the X mode waves with frequencies close to the cyclotron frequency may have group velocities much smaller than the speed of light, a feature different from that of O mode. Consequently, the spatial amplification of the X mode is more effective than the O mode, even if both have the same temporal growth rates.

A shortcoming of the preceding works (Wu and Lee, 1979; Lee et al., 1980) was pointed out by Wu (1980). In order to demonstrate that an electromagnetic cyclotron instability can exist we have considered an effective loss-cone distribution which varies with  $v_{\perp}$  according to the following functional form

$$F \sim \left( \frac{v_{\perp}^2}{\alpha^2} \right)^l \exp \left( - \frac{v_{\perp}^2}{\alpha^2} \right) \quad (1)$$

Expression (1) is frequently considered in plasma physics to investigate stability problems concerning charged particles confined in a magnetic mirror. The index  $l(l \geq 1)$  measures the steepness of the gradient  $\partial F / \partial v_{\perp}$  of an effective loss-cone distribution. Such a distribution

is, however, significantly different from observed magnetospheric loss-cone distributions which are discussed in Section II. The question which arises naturally is whether the two types of distribution functions can lead to qualitatively different conclusions (within the context of linear stability analyses). Furthermore, the realistic loss-cone distribution can be significantly modified when there is a parallel electric field below or at the site of observation. The electric field tends to broaden the loss-cone near  $v_{\parallel} = 0$  and therefore can affect the calculation of the temporal growth rate.

Another generalization of the preceding works is desirable. That is, previously we have assumed that the density of the backscattered electrons is much higher than that of the keV electrons. This assumption enables us to calculate the dispersion relation by ignoring the energetic electrons, which only contribute to the amplification of the radiation. However, at high altitudes ( $> 1 R_E$ ) few backscattered electrons (except those that can attain energies in the keV range) can reach that height without being reflected by the decreasing electrostatic potential associated with the parallel electric field. (Here we have implicitly postulated that the potential drop below the altitude of one  $R_E$  is of the order of one kilovolt or more.) If this conjecture is true, the assumption that the density of the backscattered electrons is high must be relaxed. In this case both the dispersion relation and the stability of the radiation are determined by the energetic electrons. Hence, the stability analysis becomes more complicated than that presented by Lee et al. (1980).

In view of the aforementioned considerations, a series of investigations have been carried out. The purpose of this paper is to discuss these studies and to present the relevant results. The organization of the paper is described as follows. In Sec. II we discuss the physical model on which

the stability analysis is carried out. The formulation of the stability theory is reported in Sec. III. Finally, Sec. IV presents numerical results and discussion.

## II. PHYSICAL MODEL

It is appropriate to first discuss the physical model to be considered before analyzing the stability problem. There are several basic considerations which are discussed separately as follows.

### A. Model Distribution Function Based on Spacecraft Observations

The most applicable observational results available now are those acquired with the S3-3 satellite, which has been operative in the apparent source region of AKR. Particle distribution functions are measured by the S3-3 spacecraft in the auroral acceleration region at various altitudes below about 8,000 kilometers (Mizera and Fennell, 1977; Croley et al., 1978; Fennel and Gorney, 1980). Because the *in situ* measurements of the auroral electron distribution functions provide valuable information which can be the basis of our theoretical model, a brief discussion of the observational results is not only relevant but also pertinent.

Figure 1 shows typical inverted-V signatures as observed by S3-3. This particle-wave spectrogram from Day 237, 1976 shows electron and ion differential energy flux from 0.2 - 30 keV and .09 - 3.9 keV, respectively. Also shown in the upper panel is the AC electric field amplitude (Mozer et al., 1977) with frequencies of .03 - 100 KHz. (Note that S3-3 is not capable of making in situ observations of AKR because the high-frequency cutoff of the AC electric field detector lies below the local electron gyrofrequency everywhere along the spacecraft trajectory.) In this example the spacecraft encounters several inverted-V structures between 69.8° and 74.5° invariant latitude. Electron acceleration to several kilovolts and ion acceleration to 1 - 3 keV are observed throughout this region.

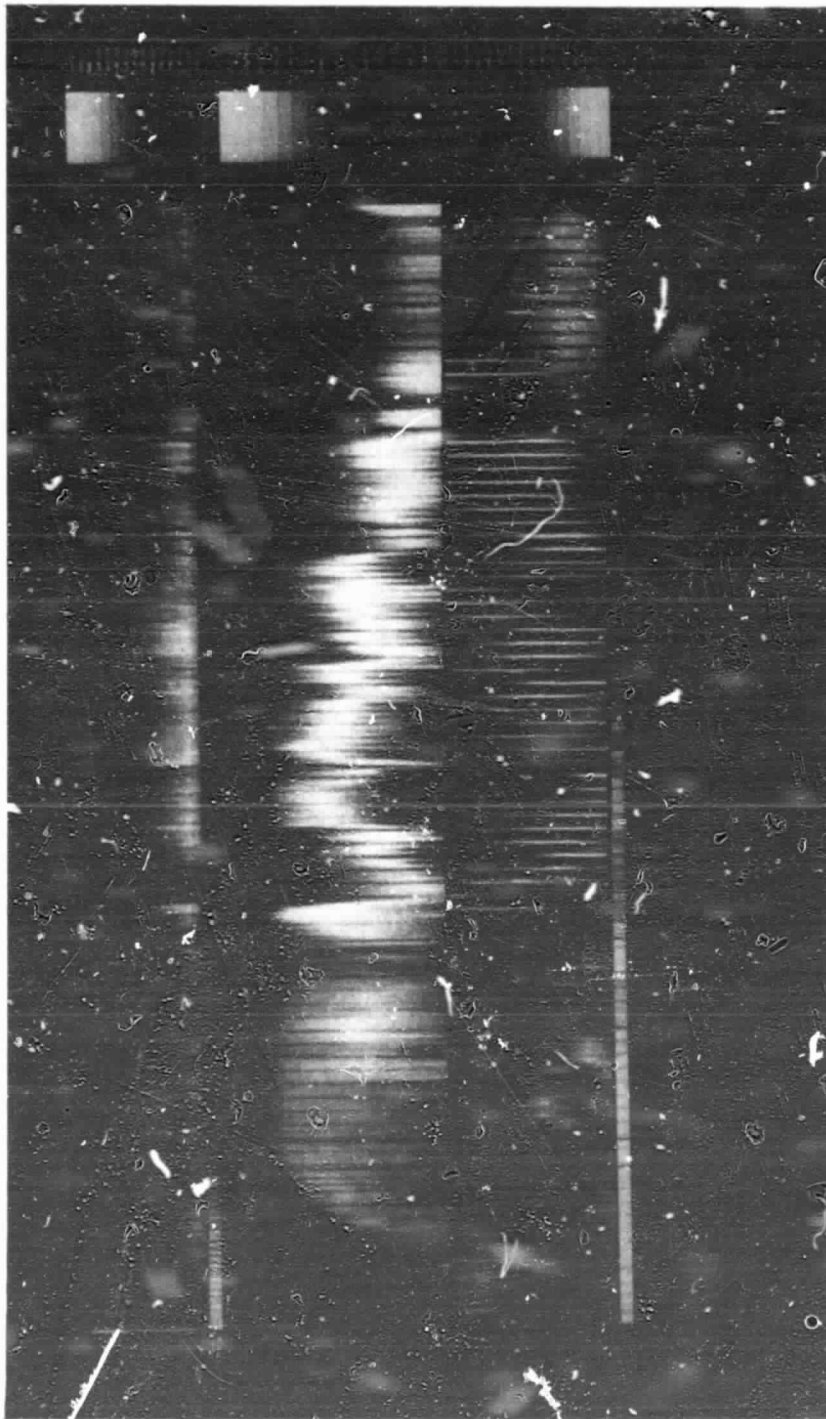


Fig. 1. S3-3 Particle-Wave Spectrogram from Day 237, 1976. Electron energy flux for  $0.2 < E < 30$  keV is shown in the center panel and ion energy flux for  $0.09 < E < 3.9$  keV is shown in the bottom panel; ac electric field amplitude (Mozer et al., 1977) in the frequency range  $0.03 - 100$  kHz is shown in the upper panel.

For the purpose of illustration we present a distribution function which was measured at 17473 seconds UT (Fig. 21.) The  $+v_{\parallel}$  axis corresponds to downgoing electrons and the  $-v_{\parallel}$  axis to upcoming electrons observed at the spacecraft. There are several interesting features. First, overall the distribution function is fairly isotropic outside the loss-cone region. Second, the loss-cone region for the upcoming electrons is partially filled. Third, the loss-cone distribution appears to be modified by a parallel electric field. Fourth, a population of trapped electrons appears to be in existence. [The definition of trapped electrons may be found in the article by Chiu and Schulz (1978)].

Based on the observations, we consider in the subsequent discussion a model distribution function of the following form

$$\begin{aligned}
 F_e &= A \exp\left(-\frac{v^2}{\alpha^2}\right) & \text{for } v_{\perp}^2 \geq \frac{v_{\parallel}^2 + \phi}{b} \\
 &= 0 & \text{for } v_{\perp}^2 < \frac{v_{\parallel}^2 + \phi}{b}
 \end{aligned} \tag{2}$$

where  $A$  is a normalization constant,  $\phi$  and  $b$  are two positive numbers which are determined by the potential difference and the mirror effect,

$$\phi \equiv \frac{2|e|(\phi_1 - \phi)}{m_e} \quad \text{and} \quad b \equiv \frac{B_{\max}}{B} - 1 \tag{3}$$

( $\phi_1$  and  $B_{\max}$  are the electrostatic potential and magnetic field at the mirror point, respectively). In the context of the inverted-V structure itself, the quantity  $\phi_1 - \phi$  represents the potential drop between the atmosphere and the point of observation. This can be estimated by measuring the ion beam energy on the enhancement in the upcoming loss-cone angle (see Mizera et al., 1981). The step-function approximation is justifiable, if the velocity spread at the loss-cone boundary is small in comparison



ORIGINAL PAGE IS  
OF POOR QUALITY

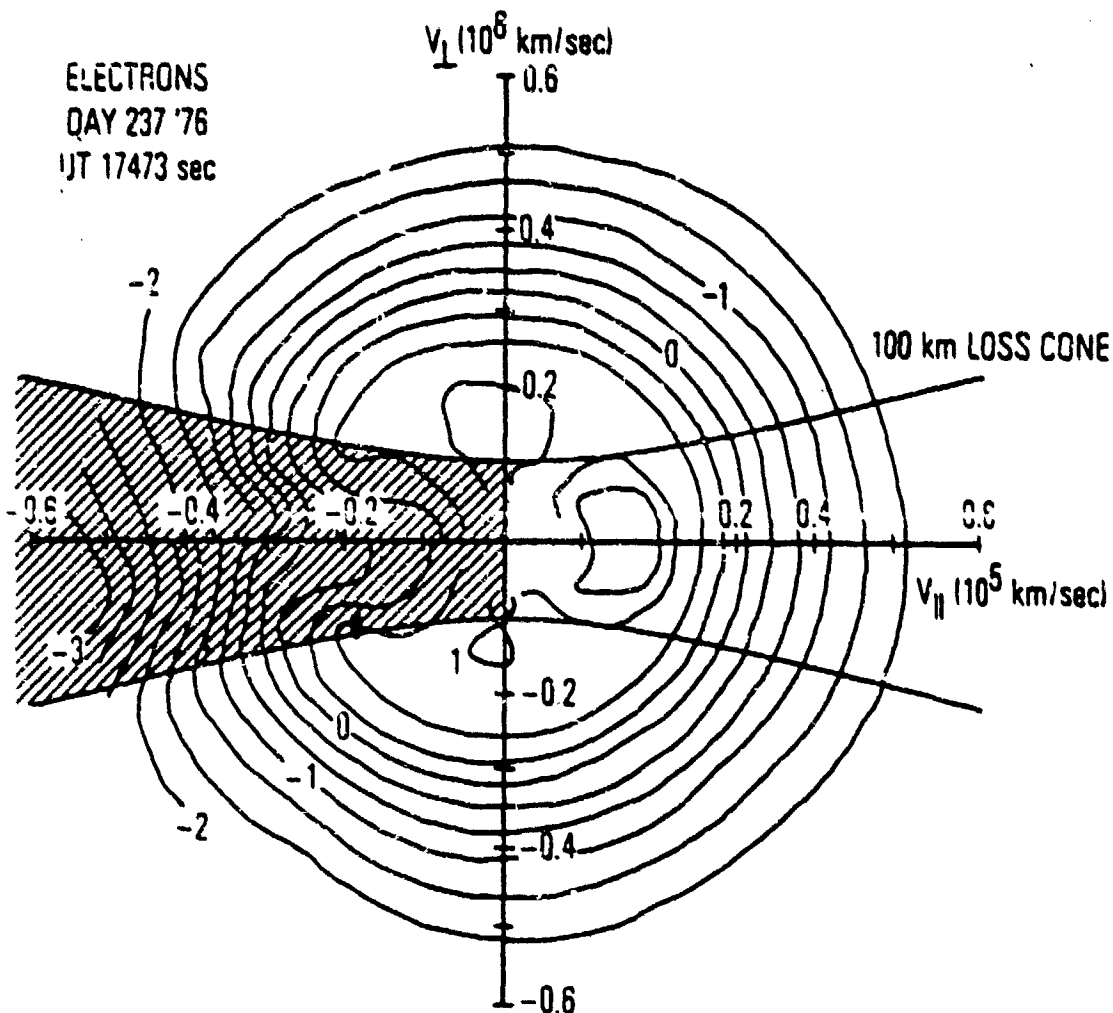


Fig. 2. An Electron Velocity-Space Distribution Taken at 17473 Seconds UT on Day 237, 1976. The  $+v_{\parallel}$  axis corresponds to downgoing particles and the  $-v_{\parallel}$  axis corresponds to upcoming particles. The 100-km loss cone, corrected for parallel potential drop beneath the point of observation, is shaded.

with the random velocity. If we require

ORIGINAL PAGE IS  
OF POOR QUALITY

$$\int d^3v F_e = 1$$

it can be shown that

$$A = \frac{1}{\pi^{3/2} \alpha^3} \left( 1 + \frac{1}{b_m} \right)^{1/2} \exp \left( -\frac{\psi}{\alpha^2 b_m} \right) \quad (4)$$

At this point a couple of comments are appropriate. Obviously, we have not included the trapped electrons. Of course, if the parallel electric field only occurs below the site of observation, the trapping process need not be considered anyway. The main reason is for simplicity. Another feature which we have not taken into account in Eq. (2) is that the downgoing electrons some time can form a beam. This point should not pose any problem, because in our analysis waves are considered to have a parallel component of the wave vector  $k_{\parallel}$  pointing upward and these waves can only resonate with the upgoing electrons. In short, the functional form of the distribution with  $+v_{\parallel}$  is unimportant for the stability problem of interest to us. For the same reason, the feature of a double loss-cone displayed by Eq. (2) should not concern us even though we are interested in the real situation in which only the upgoing electrons possess a loss-cone distribution.

#### B. Magnetic Field and Electron Density

The model distribution function described by Eq. (2) does depend upon the local value of  $b$  ( $b \equiv B_{\text{max}}/B - 1$ ). Thus a magnetic-field model is needed, before we can proceed further. Figure 3 describes a model considered in the present study. The magnetic field strength is expressed in terms of the electron cyclotron frequency,  $\omega_c (= |e|B/m_e c)$ , which is plotted versus altitude. In the same figure several local loss-cone angles are indicated for various altitudes. In this calculation

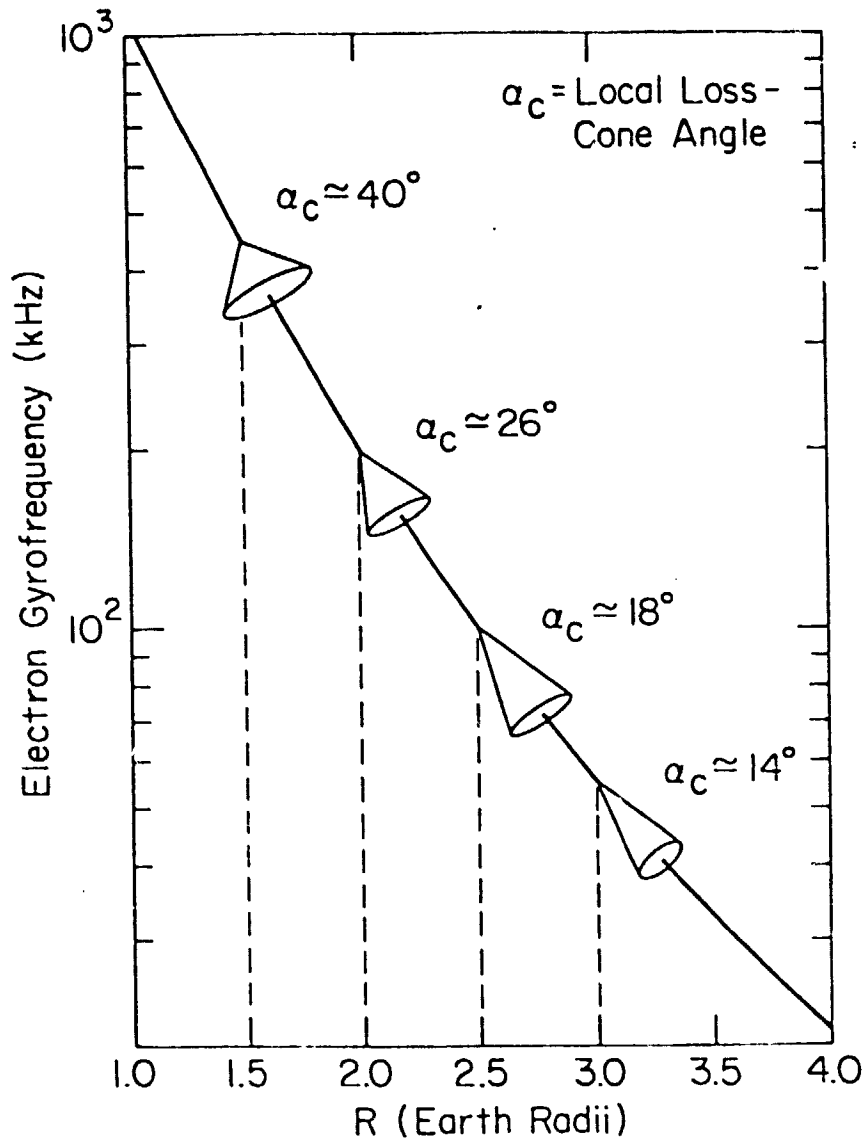


Fig. 3. Plot Showing the Dependence of Electron Gyrofrequency and Loss Cone Angle on Altitude Along Auroral Field Lines.

we have considered  $B_{\max} \approx 0.4$  Gauss.

Concerning the electron densities we consider three models. In the following we restrict our discussion to the altitudes ranging from 4000 km to 8000 km. Of course, doing this does not necessarily mean that we are assuming that AKR cannot occur outside this region. In fact, ISIS-1 observations indicate clearly that generation of AKR can take place below 4000 km (Benson and Calvert, 1979; Benson et al., 1980; Calvert, 1981). However, the general opinion is that the  $4 \times 10^3 - 8 \times 10^3$  km altitude range along the auroral field lines probably marks the most active source region of AKR. In Table 1, the three density models are described. In the same table we also list the values of the local electron gyro-frequency and the corresponding ratios  $\omega_{pe}^2 / \Omega_e^2$  where  $\omega_{pe}$  denotes the local electron plasma frequency. In Fig. 4 we plot the local values of  $\Omega_e$  and  $\omega_{pe}$  as functions of the altitude. At a given altitude, there are three values of  $\omega_{pe}$  for different density models. We note here that  $\omega_{pe}$  is determined by the total electron density (i.e.,  $n_b + n_e$ ,  $n_b$  and  $n_e$  are the density of the backscattered electrons and that of the energetic electrons, respectively).

### C. Parallel Electric Field

The parallel electric field which exists in the auroral acceleration region has been suggested and observed. However, the typical structure and distribution of such a field or fields still represent a controversial subject. A variety of possibilities have been suggested, as reviewed by Shawhan et al. (1978). Later the subject was further discussed by Chiu and Schulz (1978), Kan, et al. (1979), and many others from a theoretical point of view.

Recent observations (c.f. Fennell and Gorney, 1980) suggest that the auroral potential drop can assume a variety of distributions in altitude. We therefore have considered some simple models. Since our main interest is to investigate how the presence of a parallel electric field affects the generation of AKR, we have chosen to limit our study, for the purpose of this

ORIGINAL PAGE IS  
OF POOR QUALITY

Table 1. Density and Magnetic Field Models

MODEL	ALTITUDE (km)	$n_b$ ( $\text{cm}^{-3}$ )	$n_e$ ( $\text{cm}^{-3}$ )	$\Omega_e$ (kHz)	$\frac{\omega_a^2}{\Omega_e^2}$	$b_m = \frac{B_{\max}}{B} - 1$
D1	4,000	40	5	373	0.026	2.5
	5,000	25	5	281	0.031	3.7
	6,000	20	5	216	0.033	5.1
	7,000	15	5	170	0.056	6.8
	8,000	10	5	135	0.066	8.7
D2	4,000	30	5	373	0.020	2.5
	5,000	15	5	281	0.020	3.7
	6,000	10	5	216	0.026	5.1
	7,000	5	5	170	0.028	6.8
	8,000	3	5	135	0.035	8.7
D3	4,000	40	5	373	0.003	2.5
	5,000	20	5	281	0.005	3.7
	6,000	0	5	216	0.009	5.1
	7,000	0	5	170	0.014	6.8
	8,000	0	5	135	0.022	8.7

ORIGINAL PAGE IS  
OF POOR QUALITY

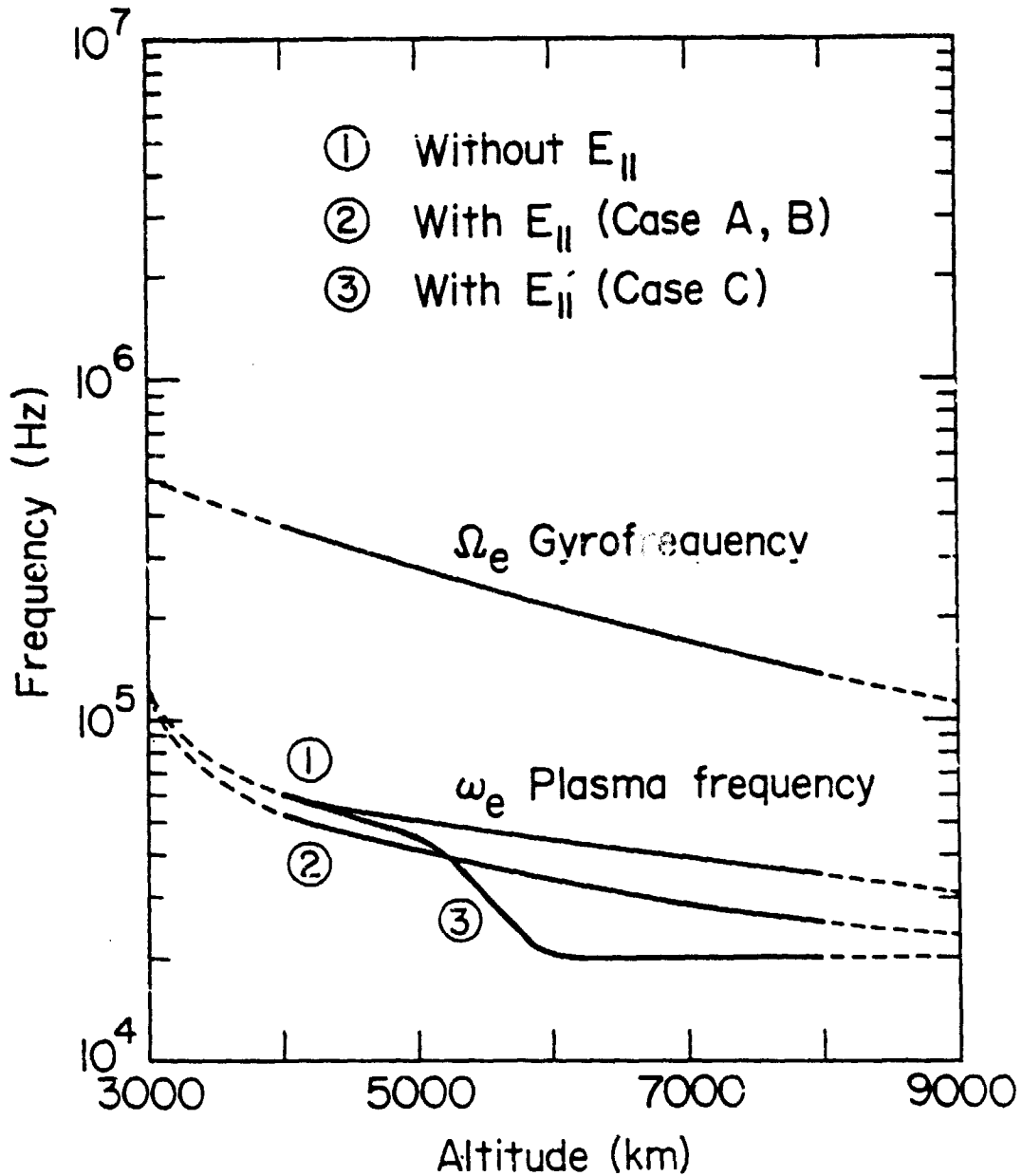


Fig. 4a. Plot Showing the Modeled Dependence of the Electron Plasma Frequency for the Altitude Range of Interest.

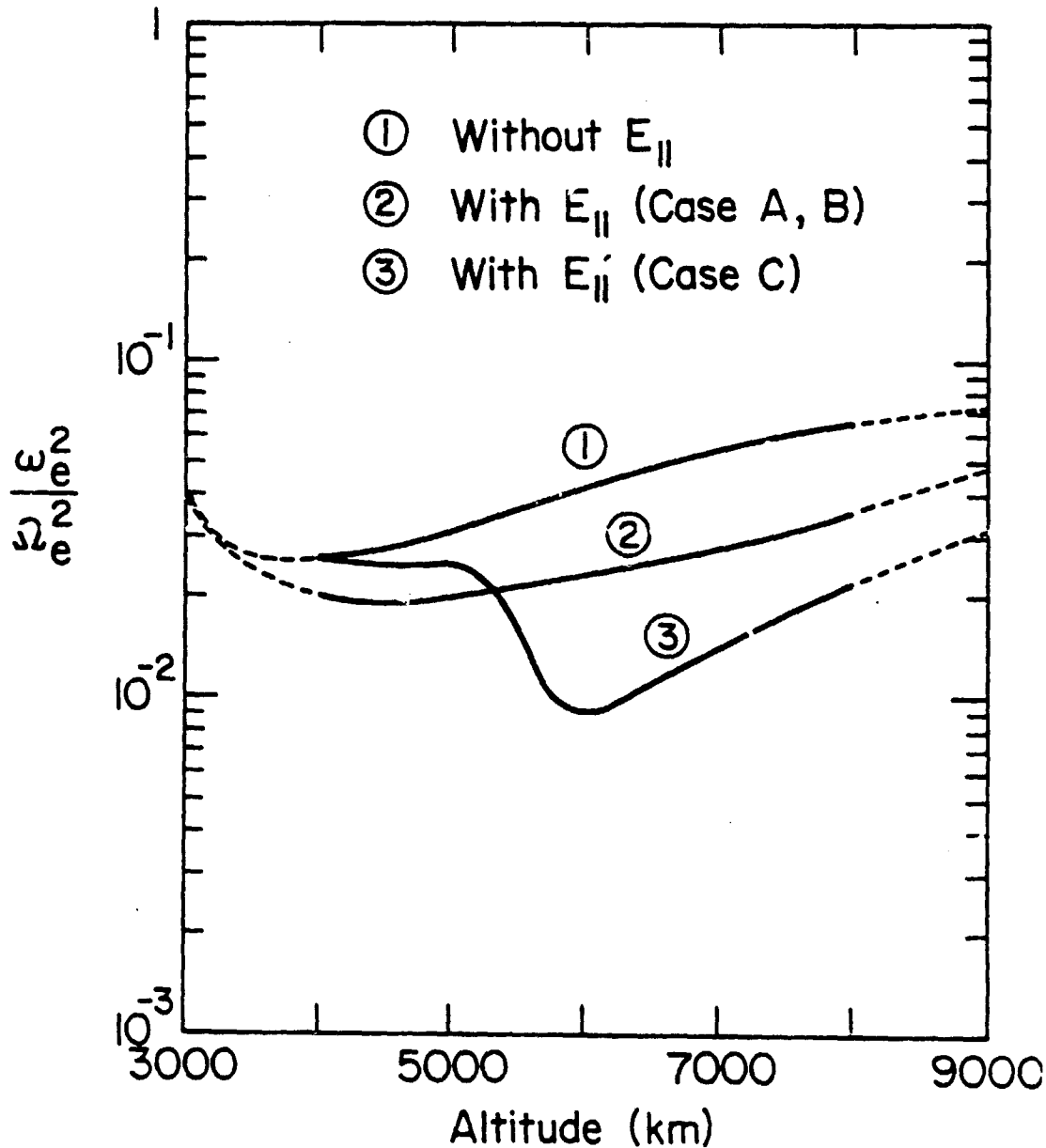


Fig. 4b. Same as Fig. 4a, but Showing the Dependence of the Ratio of the Squares of the Plasma Frequency to the Electron Gyrofrequency.

paper, to two fairly extreme models. These two models are displayed in Fig. 5 and numerical values are given in Table 2. The first model assumes that the parallel electric field is distributed over a broad altitude range, while the second model assumes a narrow potential structure with potential drop only above 4000 km.



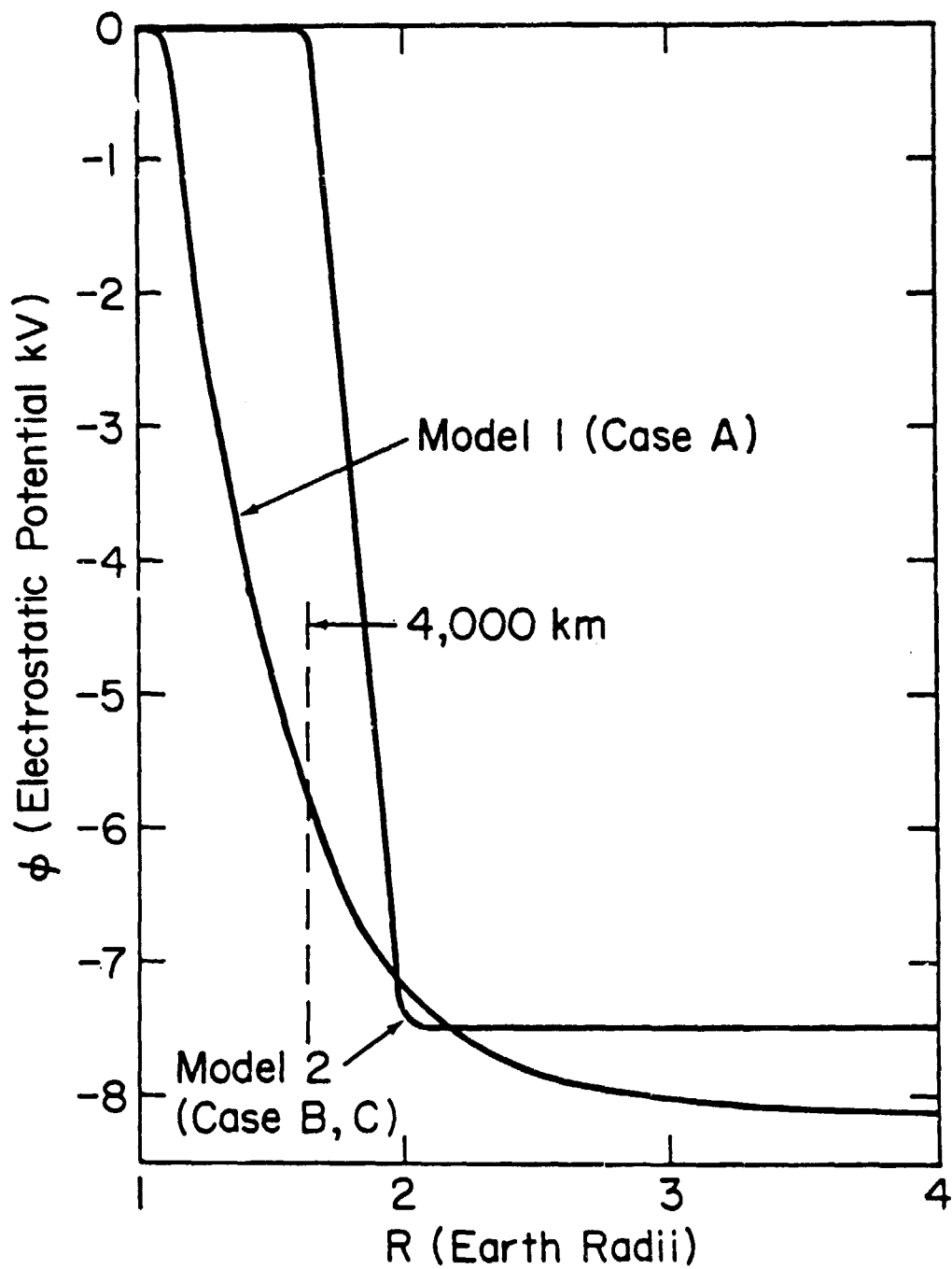


Fig. 5. Plot of the Two Potential Distribution Models used in the Wave Growth Calculations. Model 1 depicts a fairly broad potential distribution in altitude, while Model 2 contains a potential drop confined to  $\sim 3000$  km.

Table 2. Models of the Parallel Electric Field and Auroral-Electron Energies

MODEL	ALTITUDE (km)	$\frac{\alpha^2}{c^2} \times 10^2$	$\frac{\phi}{c^2} \times 10^2$
E1	4,000	1.72	2.28
	5,000	1.38	2.62
	6,000	1.17	2.83
	7,000	1.05	2.95
	8,000	0.97	3.03
E2	4,000	4.0	0.0
	5,000	2.0	2.0
	6,000	1.0	3.0
	7,000	1.0	3.0
	8,000	1.0	3.0

### III. DISPERSION EQUATION

In order to study the amplification of the radiation we want to investigate the dispersion equation which can be derived from linearized Vlasov equations and is well known in the literature of plasma physics. The general form of the dispersion equation is complicated if the plasma is magnetized and the perturbation has mixed electrostatic and electromagnetic polarization. Furthermore, if the wave frequency of interest is close to the electron cyclotron frequency or its harmonics, the relativistic effect on the mass of the resonant electrons may be important, even for keV electrons. In this case, the solution of the dispersion equation is not easily obtainable. The problem is somewhat simplified when the low-energy background electrons have a density dominant over that of the energetic electrons. In this case the real part of the wave frequency is predetermined by the background electrons. Such an approximation has been considered by Lee et al. (1980), but it is not generally valid, as discussed earlier. Nevertheless, the approximate expressions for growth rates given either by Wu and Lee (1979) or by Lee et al. (1980), contain a piece of very essential information. That is, the resonant condition between the wave and electrons becomes qualitatively different when the relativistic effect is included. A discussion of this point is not only relevant, but highly important. This is the purpose of Subsection III. A.

Mathematically the relativistic effect also complicates the calculation of the dielectric tensor. Usually, when the relativistic effect is neglected, the integration with respect to  $v_{\perp}$  can be carried out for a certain class of non-equilibrium (unperturbed) distribution functions. The inclusion of the relativistic effect makes the  $v_{\perp}$

integration very difficult, if not impossible. However, one may adopt an approach different from the conventional method of calculating the dielectric tensor. This point is presented in Subsection III. B.

Finally, the dispersion equation of interest to us is presented in subsection III. C. The equation is expressed in terms of a number of integrals in  $\tau$  (time) space. Eventually we have to use numerical method to obtain the solution of this dispersion equation.

#### A. Resonance Condition

From Wu and Lee (1979) and Lee et al. (1980), we see that a resonance condition

$$\omega_r - \Omega_e \left( 1 - \frac{v^2}{2c^2} \right) - k_{\parallel} v_{\parallel} = 0 \quad (5)$$

plays an essential role in the determination of the temporal growth rate.

(Here, the approximation of weakly relativistic electrons has been applied.)

This condition can be rewritten as

$$\frac{v_{\perp}^2}{c^2} + \left( \frac{v_{\parallel}}{c} - \frac{\omega_r}{\Omega_e} N \cos \theta \right)^2 = \frac{\omega_r^2}{\Omega_e^2} N^2 \cos^2 \theta - 2 \left( \frac{\omega_r}{\Omega_e} - 1 \right) \quad (6)$$

where  $\cos \theta = k_{\parallel}/k$ ;  $N = kc/\omega_r$  is the index of refraction;  $\omega_r$  denotes the wave frequency and  $\Omega_e = |e|B_0/m_e c$  is the electron cyclotron frequency. The resonant velocities can be readily plotted, as shown in Fig.

6. Clearly, the geometrical configuration is a circle which is centered at  $v_{\parallel} = c(\omega_r N \cos \theta / \Omega_e)$  and has a radius  $R = [(\omega_r^2 N^2 \cos^2 \theta / \Omega_e^2) - 2(\omega_r / \Omega_e - 1)]^{1/2}$ . Evidently, the discussion is meaningful only when

$$\frac{\omega_r^2}{\Omega_e^2} N^2 \cos^2 \theta > 2 \left( \frac{\omega_r}{\Omega_e} - 1 \right).$$

ORIGINAL PAGE IS  
OF POOR QUALITY

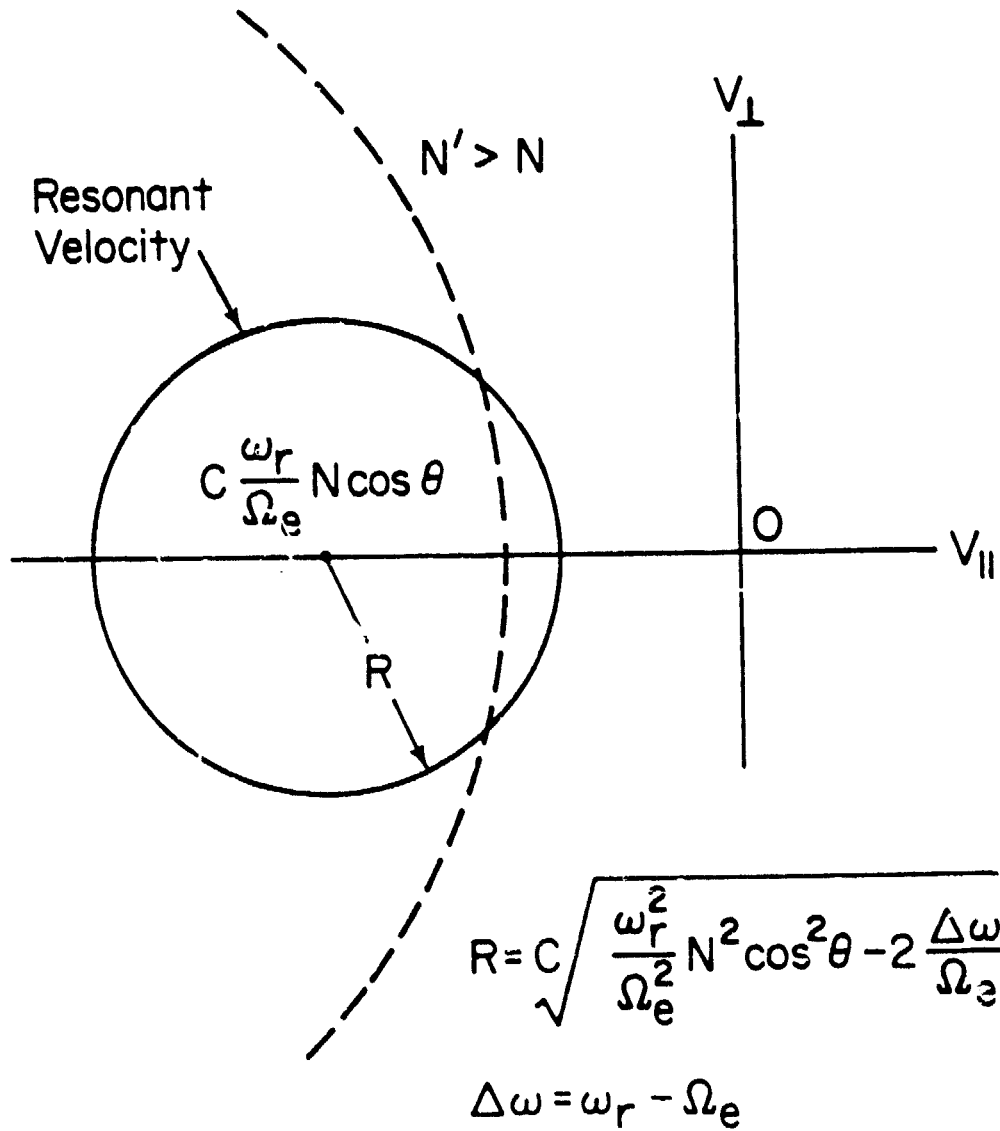


Fig. 5. Schematic Plot Showing the Shape of the Relativistic Resonant Surface for the Extraordinary Mode. The radius of the resonance circle is shown in the inset.

Clearly, for  $\omega_r = \Omega_e$ , the circle does not enclose the origin. One can easily envision that when  $N \rightarrow \infty$  and  $v^2 \ll c^2$ , the resonant circle degenerates into a straight line

$$v_{\parallel} k \cos \theta = \left( \frac{\omega_r}{\Omega} - 1 \right) \quad (7)$$

which describes the usual Doppler effect and normal cyclotron resonance. The pertinent point here is that when  $\omega_r = \Omega_e$ ,  $N \cos \theta < 1$  and  $v/c < 1$ , all terms in Eq. (6) may be of the same order of magnitude. In that case the neglect of the relativistic effect in Eq. (5) is not justified.

Moreover, it is seen that the inclusion of the relativistic term in the resonance condition tends to limit the resonant velocities to small  $v_{\perp}$  or

$$v_{\perp} < c \left[ \frac{\omega_r^2}{\Omega_e^2} N^2 \cos^2 \theta - 2 \left( \frac{\omega_r}{\Omega} - 1 \right) \right]^{\frac{1}{2}}$$

whereas the usual resonance condition described by Eq. (7) is independent of  $v_{\perp}$ , meaning electrons with arbitrary  $v_{\perp}$  can interact with the wave as long as  $v_{\parallel}$  satisfies Eq. (7). Consequently, for a given unperturbed distribution the two resonance conditions can lead to qualitatively different results, similar in stability analyses. For instance, the former condition leads to the conclusion that electromagnetic waves may be amplified if the energetic electrons possess a loss-cone type distribution and the latter cannot achieve this result. This point can be easily envisioned from the analysis presented by Wu and Lee (1979).

We shall return to this point later when we discuss the numerical results to be presented in Sec. IV.

#### B. Method of Calculating the Dielectric Tensor $\epsilon_{ij}$

Since the dispersion equation can be written in terms of the dielectric tensor  $\epsilon_{ij}(k, \omega)$ , i. e.

$$\det \left| \frac{c^2}{\omega^2} (k_i k_j - \delta_{ij} k^2) + \epsilon_{ij}(k, \omega) \right| = 0 \quad (8)$$

to obtain the expressions for the tensorial components of  $\epsilon_{ij}$  appears to be a crucial task. Hereafter we introduce the definition

$$\epsilon_{ij} = \delta_{ij} + Q_{ij}^b + Q_{ij}^e \quad (9)$$

where the superscripts  $b$  and  $e$  denote respectively the contributions from the background (or backscattered) electrons and the energetic electrons. Because the background electrons are supposed to have low energies,  $Q_{ij}^b$  may be written as

$$\begin{aligned} Q_{xx}^b &= Q_{yy}^b = -\frac{\omega_{be}^2}{\omega^2 - \Omega_e^2} \\ Q_{xy}^b &= -Q_{yx}^b = \frac{i\omega_{be}^2 \Omega_e}{\omega(\omega^2 - \Omega_e^2)^2} \\ Q_{zz}^b &= -\frac{\omega_{be}^2}{\omega^2} \\ Q_{xz}^b &= Q_{zx}^b = Q_{yz}^b = Q_{zy}^b = 0 \end{aligned} \quad (10)$$

where  $\omega_{be}^2 = 4ne^2 n_b / m_e$ . These expressions are well known in the literature and obtainable with the so-called "cold-plasma" approximation.

On the other hand, for the energetic electrons,  $Q_{ij}^e$  can be expressed as

$$\begin{aligned} Q_{ij}^e &= 2\pi \frac{\omega_e^2}{\omega^2} \int_{-\infty}^{+\infty} du_{\parallel} \int_0^{\infty} du_{\perp} \frac{u_{\parallel}}{\gamma} \left( u_{\perp} \frac{\partial}{\partial u_{\parallel}} - u_{\parallel} \frac{\partial}{\partial u_{\perp}} \right) F_e \hat{e}_z \hat{e}_z \\ &+ 2\pi \frac{\omega_e^2}{\omega^2} \int_{-\infty}^{+\infty} du_{\parallel} \int_0^{\infty} du_{\perp} \left[ \omega \frac{\partial}{\partial u_{\perp}} + \frac{k_{\parallel}}{\gamma} \left( u_{\perp} \frac{\partial}{\partial u_{\parallel}} - u_{\parallel} \frac{\partial}{\partial u_{\perp}} \right) \right] F_e(u) \\ &\times \sum_{n=-\infty}^{\infty} \frac{\Gamma_{ij}^{(n)}}{\gamma\omega - n\Omega_e - k_{\parallel}u_{\parallel}} \end{aligned} \quad (11)$$

where  $\Omega_e = |eB_0/m_e c|$ ;  $\omega_e = (4\pi e^2 n_e / m_e)^{1/2}$  is the plasma frequency of the energetic electrons;  $F_e$  is the unperturbed distribution function of the energetic electrons; and the tensor  $T_{ij}^{(n)}$  is given by

$$T_{ij}^{(n)} = \begin{pmatrix} \frac{n^2 \Omega_e^2}{k_{\perp}^2} J_n^2 & -\frac{i n \Omega_e}{k_{\perp}} u_{\perp} J_n J_n' & +\frac{n \Omega_e}{k_{\perp}} u_{\parallel} J_n^2 \\ +\frac{i n \Omega_e}{k_{\perp}} u_{\perp} J_n J_n' & u_{\perp}^2 J_n'^2 & +i u_{\parallel} u_{\perp} J_n J_n' \\ +\frac{n \Omega_e}{k_{\perp}} u_{\parallel} J_n^2 & -i u_{\parallel} u_{\perp} J_n J_n' & u_{\parallel}^2 J_n^2 \end{pmatrix} \quad (12)$$

where  $J_n = J_n(k_{\perp} u_{\perp} / \Omega_e)$ .

In Eq. (11) for convenience we have used the momentum per unit mass  $\underline{u} \equiv \underline{p}/m_e$  ( $m_e$  is the rest mass of an electron and  $\underline{p}$  is the electron momentum) instead of  $\underline{v}$ , the electron velocity. Correspondingly, we have  $\gamma = (1 + u^2/c^2)^{1/2}$  which is the relativistic factor. Since we are merely interested in waves with  $\omega = \Omega_e$ , we need only to retain  $n=+1$  and 0 terms in Eq. (11). Moreover, because the auroral electrons have energies about several keV, it can be shown that the argument of the Bessel function  $J_{\pm 1}$  is smaller than unity. Thus we may use the following approximate expressions:

$$\begin{aligned} T_{xx}^{(+1)} &= T_{yy}^{(+1)} = \frac{u_{\perp}^2}{4} \\ T_{zz}^{(+1)} &= \frac{k_{\perp}^2 u_{\perp}^2}{4 \Omega_e^2} u_{\parallel}^2 \\ T_{xy}^{(+1)} &= +i \frac{u_{\perp}^2}{4} = -T_{yx}^{(+1)} \\ T_{xz}^{(+1)} &= +\frac{k_{\perp} u_{\perp}}{4 \Omega_e} u_{\perp} u_{\parallel} = T_{zx}^{(+1)} \end{aligned}$$

ORIGINAL PAGE IS  
OF POOR QUALITY



$$T_{yz}^{(+1)} = \pm i \frac{k_{\perp} u_{\perp}}{4\pi \epsilon_0} u_{\perp} u_{\parallel} = - T_{zy}^{(+1)}$$

Because the mean electron energy is low, the relativistic effect is expected to be weak. It is apparent that only the effect appears in the denominator;  $\gamma\omega - \Omega_e - k_{\parallel} u_{\parallel}$ . This is important, because the pole

$$\gamma\omega - \Omega_e - k_{\parallel} u_{\parallel} = 0$$

determines the resonance between the wave and electrons, as discussed earlier. Physically, this condition controls the amplification or absorption of the radiation which concerns us.

To proceed with our discussion, we remark two points. First, because we are concerned with the fast extraordinary-mode waves which have indices of refraction smaller than unity, we see that the anomalous cyclotron resonance  $\gamma\omega + \Omega_e - k_{\parallel} u_{\parallel} = 0$  is impossible. Thus the  $u_{-}$  integral which appears in the expression for  $Q_{ij}^{\bullet}$ , associated with  $n=-1, 0$ , may be again discussed in the "cold-electron" limit. Second, the term associated with  $n = 1$  can be studied by first writing (Tsai et al., 1981)

$$\frac{1}{\gamma\omega - \Omega_e - k_{\parallel} u_{\parallel}} = \frac{1}{i} \int_0^{\infty} dt \exp [i(\gamma\omega - \Omega_e - k_{\parallel} u_{\parallel})t]$$

We find that subsequently the  $u_{-}$  integration can be performed, if  $F_e$  is a loss-cone distribution as described by Eq. (2). The details are presented in a separate article (Wong et al., 1981).

C. Expression for  $Q_{ij}^e (n=1)$

After some algebraic manipulations, the aforementioned method of calculation leads us to the following expressions for  $Q_{ij}^e (n=1)$ .

$$Q_{xx}^e (n=1) = i \frac{\omega^2}{\omega^2} \frac{c^2}{\alpha^2} \exp\left(-\frac{h^2}{\mu}\right) \int_0^{\infty} d\tau \exp\left(i\bar{z}\tau + \frac{h^2}{\mu(1-i\tau)}\right) \times \left( \frac{\phi_1}{(1-i\tau)^{1/2}} + \frac{\phi_2}{(1-i\tau)^{3/2}} + \frac{\phi_3}{(1-i\tau)^{5/2}} + \frac{\phi_4}{(1-i\tau)^{7/2}} \right) \quad (13)$$

$$Q_{xz}^e (n=1) = i \frac{\omega^2}{\omega^2} \frac{c^2}{\alpha^2} \frac{k_1 \alpha}{\Omega_e} \exp\left(-\frac{h^2}{\mu}\right) \int_0^{\infty} d\tau \exp\left(i\bar{z}\tau + \frac{h^2}{\mu(1-i\tau)}\right) \times \left( \frac{g_1}{(1-i\tau)^{1/2}} + \frac{g_2}{(1-i\tau)^{3/2}} + \frac{g_3}{(1-i\tau)^{5/2}} + \frac{g_4}{(1-i\tau)^{7/2}} + \frac{g_5}{(1-i\tau)^{9/2}} \right) \quad (14)$$

$$Q_{zz}^e (n=1) = i \frac{\alpha^2}{\omega^2} \frac{c^2}{\alpha^2} \frac{k_1^2 \alpha^2}{\Omega_e^2} \exp\left(-\frac{h^2}{\mu}\right) \int_0^{\infty} d\tau \exp\left(i\bar{z}\tau + \frac{h^2}{\mu(1-i\tau)}\right) \left( \frac{f_1}{(1-i\tau)^{1/2}} + \frac{f_2}{(1-i\tau)^{3/2}} + \frac{f_3}{(1-i\tau)^{5/2}} + \frac{f_4}{(1-i\tau)^{7/2}} + \frac{f_5}{(1-i\tau)^{9/2}} + \frac{f_6}{(1-i\tau)^{11/2}} \right) \quad (15)$$

where  $\phi_j (j = 1, 2, \dots, 4)$ ,  $g_\alpha (\alpha = 1, 2, \dots, 5)$  and  $f_\beta (\beta = 1, 2, \dots, 6)$  are described in the Appendix). Moreover, we note that  $Q_{yy} = iQ_{xy} = -iQ_{yx} = Q_{xx}$  and  $Q_{xz} = Q_{zx} = iQ_{zy} = -iQ_{yz}$ .

In obtaining these expressions we have introduced the following definitions:

$$h \equiv \frac{k_1 c^2}{\omega \alpha}$$

$$\bar{z} \equiv \frac{2c^2}{\alpha^2} \left(1 - \frac{\Omega_e}{\omega}\right) + \frac{\phi}{\alpha^2 b} - \frac{h^2}{\mu} \quad (16)$$

A. Numerical Method

Evidently, the dispersion equation is complicated and very difficult to solve. In the following we use a numerical method for investigating the solution. Before going further we point out that since

$$\exp\left(\frac{h^2}{\mu(1-i\tau)}\right) = \sum_{p=0}^{\infty} \left(\frac{h^2}{\mu}\right)^p \frac{1}{\Gamma(p+1)(1-i\tau)^p} \quad (17)$$

Consequently, the tensor  $Q_{ij}^e$  ( $n=1$ ) may be expressed in terms of a function  $F_q(z)$  which is defined as

$$F_q(z) \equiv -i \int_0^{\infty} d\tau \frac{\exp(iz\tau)}{(1-i\tau)^q} \quad (18)$$

with  $q = 0, 1, 2, \dots$ . As pointed out by Shkarofsky (1966), the function  $F_q(z)$  may be written in terms of the usual plasma dispersion function  $Z$  Fried and Conte (1961), according to the relation

$$-iF_q(z) = \sum_{m=0}^{q-\frac{3}{2}} (-z)^m \frac{\Gamma(q-1-m)}{\Gamma(q)} + \frac{\pi^{1/2}}{\Gamma(q)} (-z)^{q-\frac{3}{2}} \times [iz^{1/2} Z(iz^{1/2})] \quad \text{for } q \geq \frac{3}{2} \quad (19)$$

and 
$$F_{1/2}(z) = \frac{1}{z^{1/2}} Z(iz^{1/2}) \quad (20)$$

In deriving the expressions for  $Q_{ij}^e$  we have assumed implicitly that the complex frequency  $\omega$  has a positive imaginary part. Since the analytic continuation of the  $Z$  function to the lower half of  $\omega$  plane is well known, the validity of the function  $F_q(z)$  can be extended to the entire complex plane. This consideration enables us to solve the dispersion equation by numerical method.  $Q_{ij}^e$  ( $n=-1$ ) may be approximated as

$$\approx Q^e (n=-1) = \begin{pmatrix} -\frac{\omega_e^2}{2\omega(\omega+\Omega_e)} & 1 \frac{\omega_e^2}{2\omega(\omega+\Omega_e)} & 0 \\ -1 \frac{\omega_e^2}{2\omega(\omega+\Omega_e)} & -\frac{\omega_e^2}{2\omega(\omega+\Omega_e)} & 0 \\ 0 & 0 & 0 \end{pmatrix} \quad (21)$$

Furthermore, we need to include  $Q_{zz}^e (n=0) = -\omega_e^2/\omega^2$  in the dispersion equation, because this term is of the same order of magnitude as the other terms.

### B. Results of Computation

Extensive amount of computation has been carried out. Numerical solutions of the dispersion equation are obtained for the four cases mentioned in Sec. II. In the following we present the results in Figs. 7-12.

In Fig. 7, the maximum growth rate,  $\omega_{i,max}'$  is plotted versus altitude. It is shown that in case C, the maximum growth rate is highest at altitude greater than 5000 km. This is the case in which all low-energy electrons are assumed to be removed by the parallel electric field. On the other hand, the growth rate for case D is lowest. It is seen that  $\omega_{i,max}'$  decreases rapidly above 5,000 km. At 8,000 km, it is almost two orders of magnitude smaller than that in case C. In Fig. 8, the spatial amplification distance,  $\omega_{i,max}'/v_g$  (where  $v_g$  is the corresponding group velocity), is plotted versus altitude. The distance is normalized. In case B, the spatial e-folding amplification distance is the largest in comparison with that for case D, where amplification is least effective. On the other hand, the amplification is most effective when case C is considered, as shown in Fig. 9. This result is attributed to two basic factors: one is the high temporal growth rate and the other is the small group velocity corresponding to the  $\omega_{i,max}'$

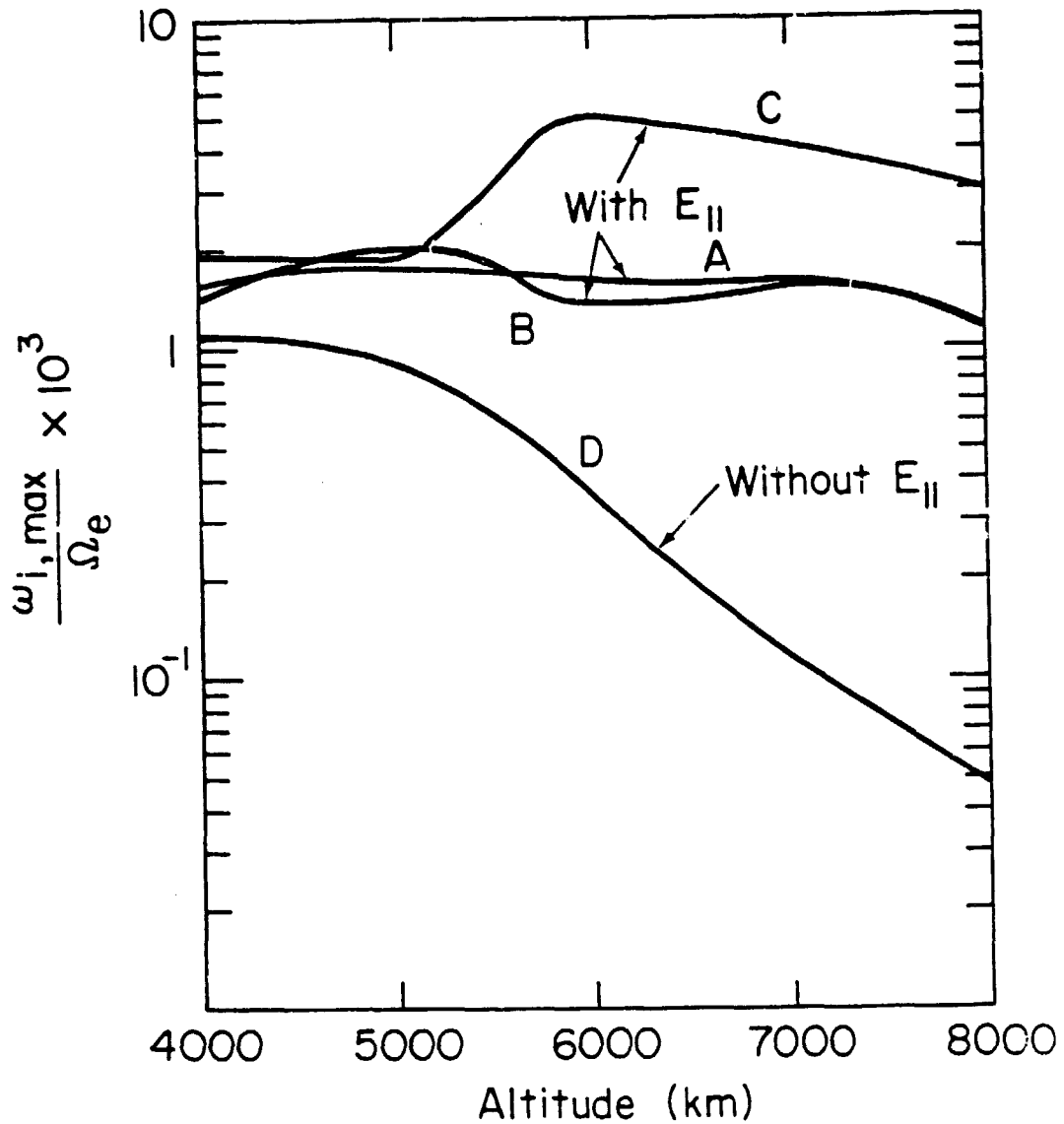


Fig. 7. Normalized Growth Rate Versus Altitude for Density Models A, B, C and D, With and Without Parallel Electric Field. (See Tables 1 and 2).

ORIGINAL PAGE IS  
OF POOR QUALITY

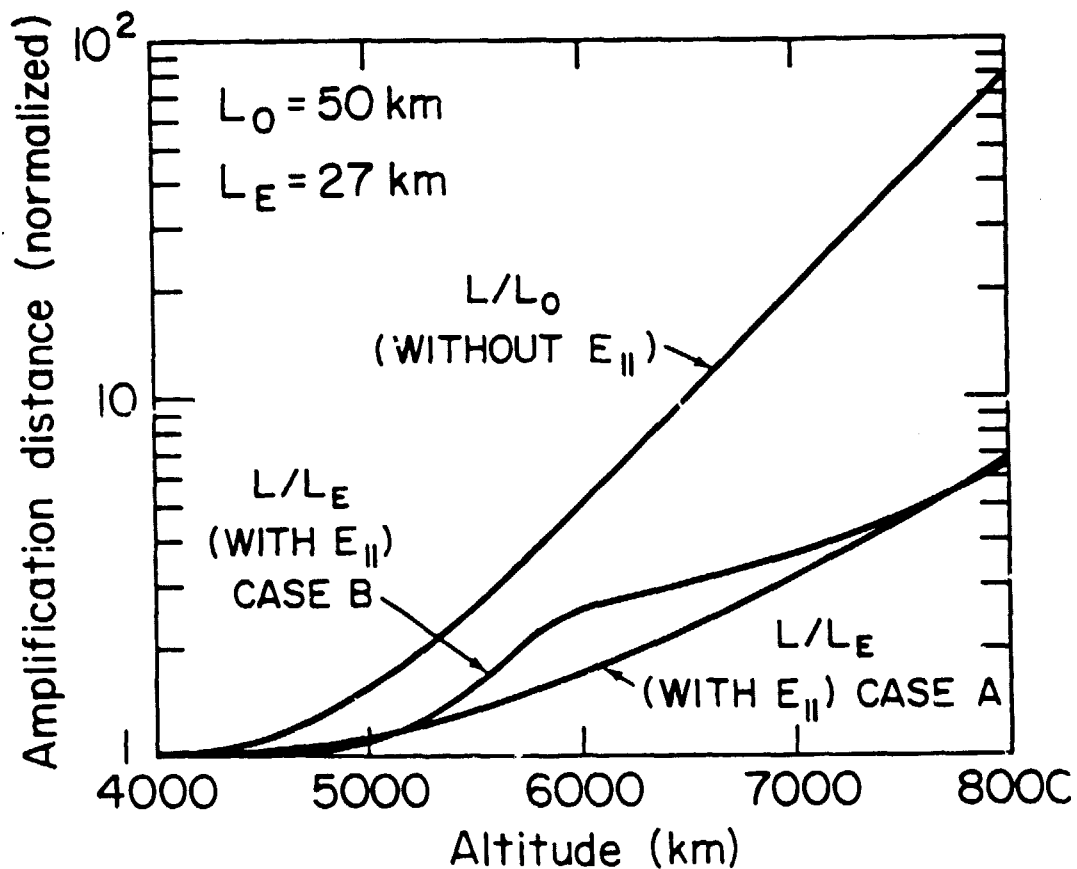


Fig. 8. Normalized Amplification Distance Versus Altitude for Models With and Without Parallel Electric Field

ORIGINAL PAGE IS  
OF POOR QUALITY

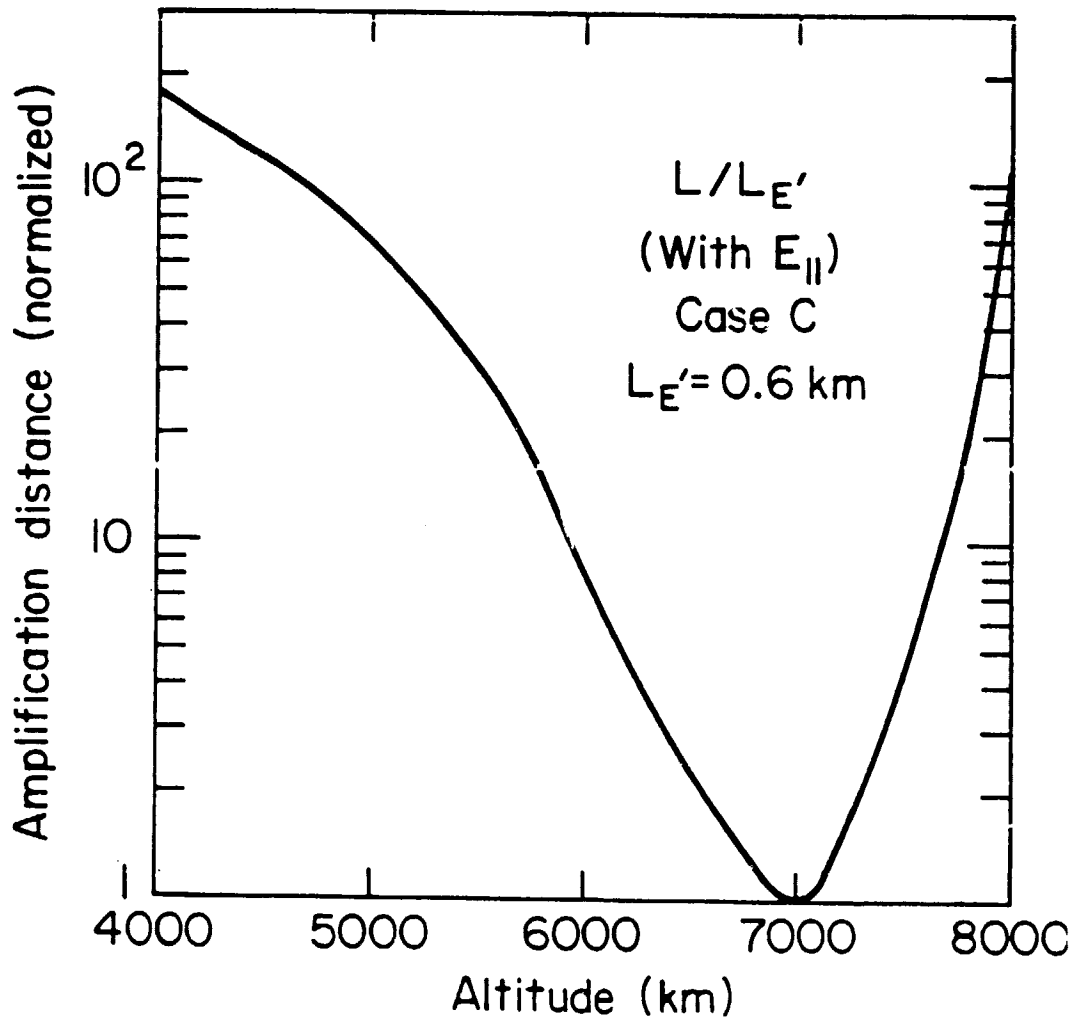


Fig. 9. Same as Fig. 8, but Depicting Case C With a Parallel Electric Field.

ORIGINAL PAGE IS  
OF POOR QUALITY

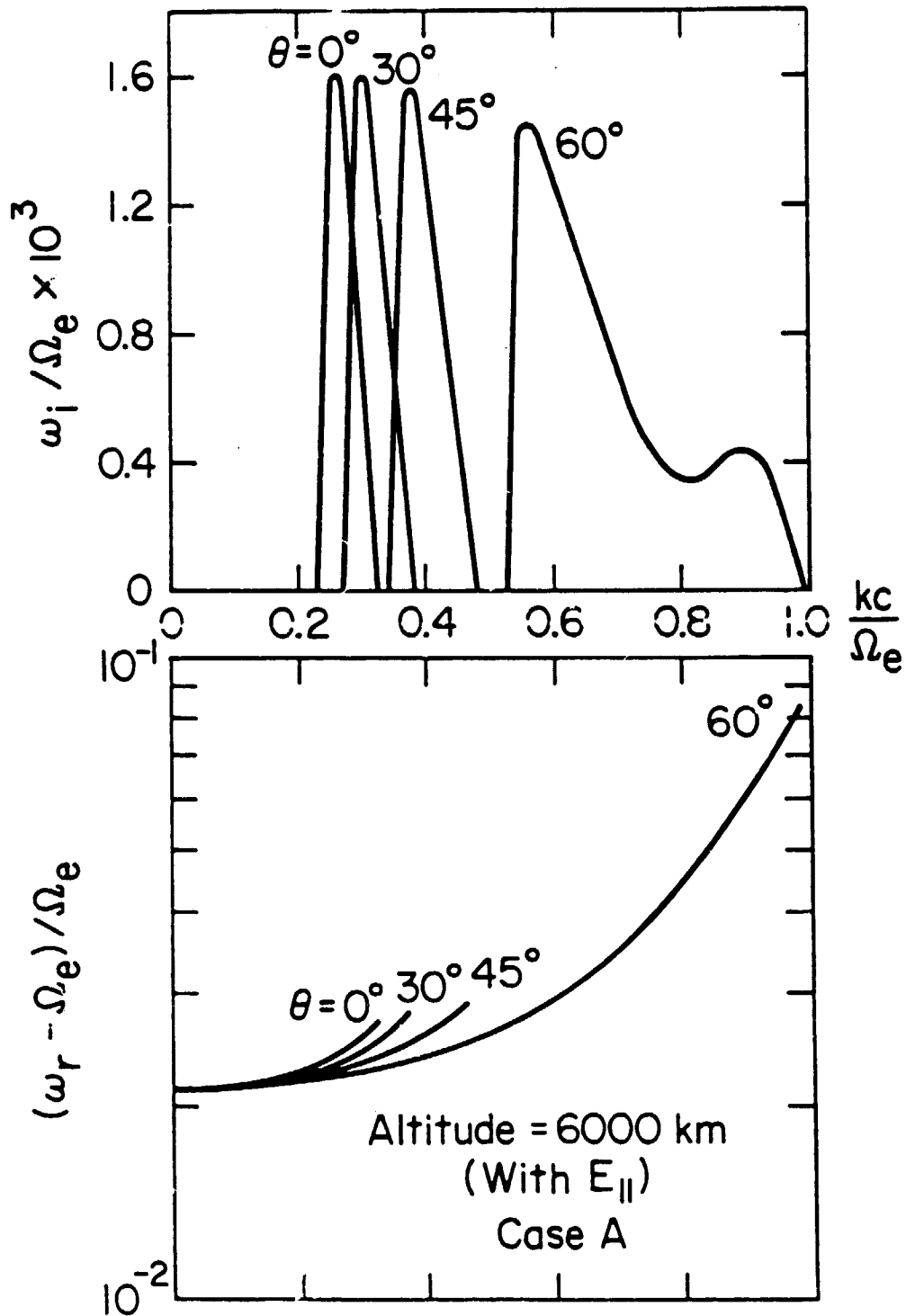


Fig. 10. Real and Imaginary Frequency Versus Wave Number for Wave Normal Angles of  $\theta = 0^\circ, 30^\circ, 45^\circ$  and  $60^\circ$ , Case A.



ORIGINAL PAGE IS  
OF POOR QUALITY

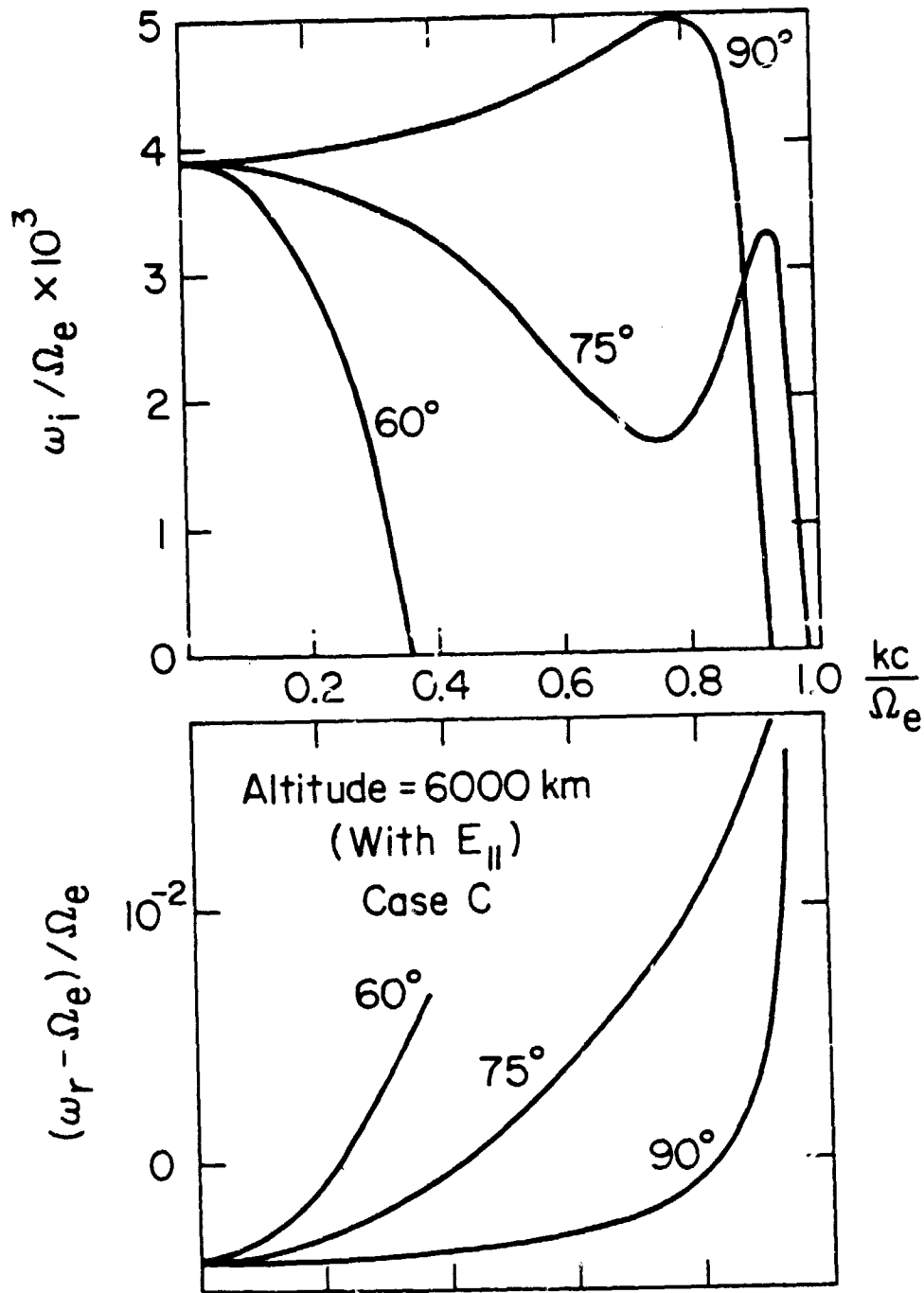


Fig. 11. Same as Fig. 10, but for Case C.

ORIGINAL PAGE IS  
OF POOR QUALITY

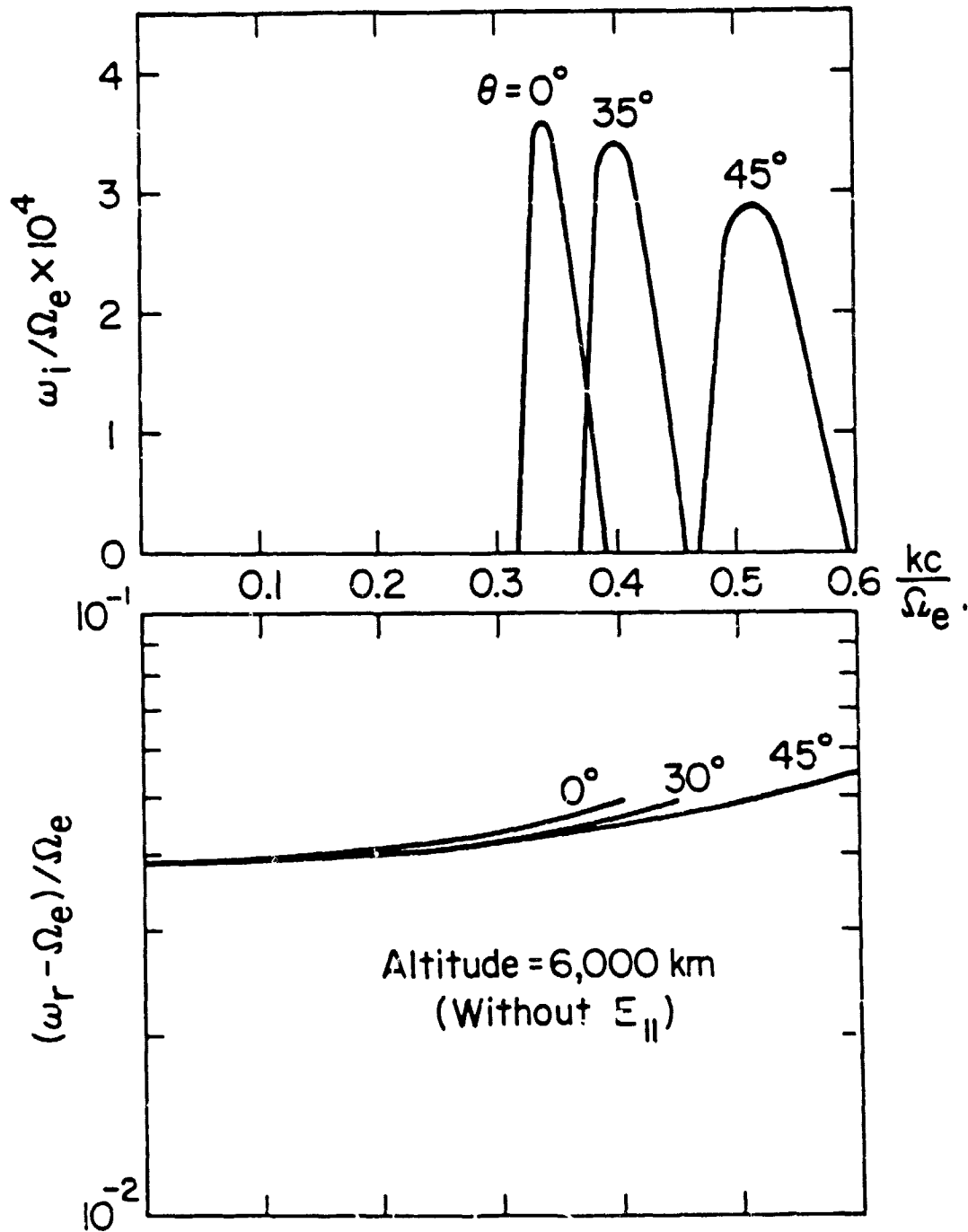


Fig. 12. Same as Fig. 10, but With No Parallel Electric Field.

We now examine the details of the solutions for cases A, B, C, and D, at 6,000 km where  $\Omega_e$  is about two hundred kHz. It is found that in case A and case B, the maximum growth rates for various  $\theta$  are somewhat similar, if  $\theta \leq 60^\circ$ . For  $\theta > 60^\circ$  the growth rate diminishes. We only present the result concerning case A. Both the growth rate  $\omega_i$  and the real frequency  $\omega_r$  are plotted in Fig. 10. The upper panel shows  $\omega_i$  as a function of  $k$ . Four values of  $\theta$  are considered. For each value of  $\theta$ , the growth rate  $\omega_i$  occurs over a certain range of  $k$ . The peak value of  $\omega_i$  shifts to higher values of the wave-number as  $\theta$  increases. In the lower panel, the real frequency  $\omega_r$  is plotted versus  $k$ .

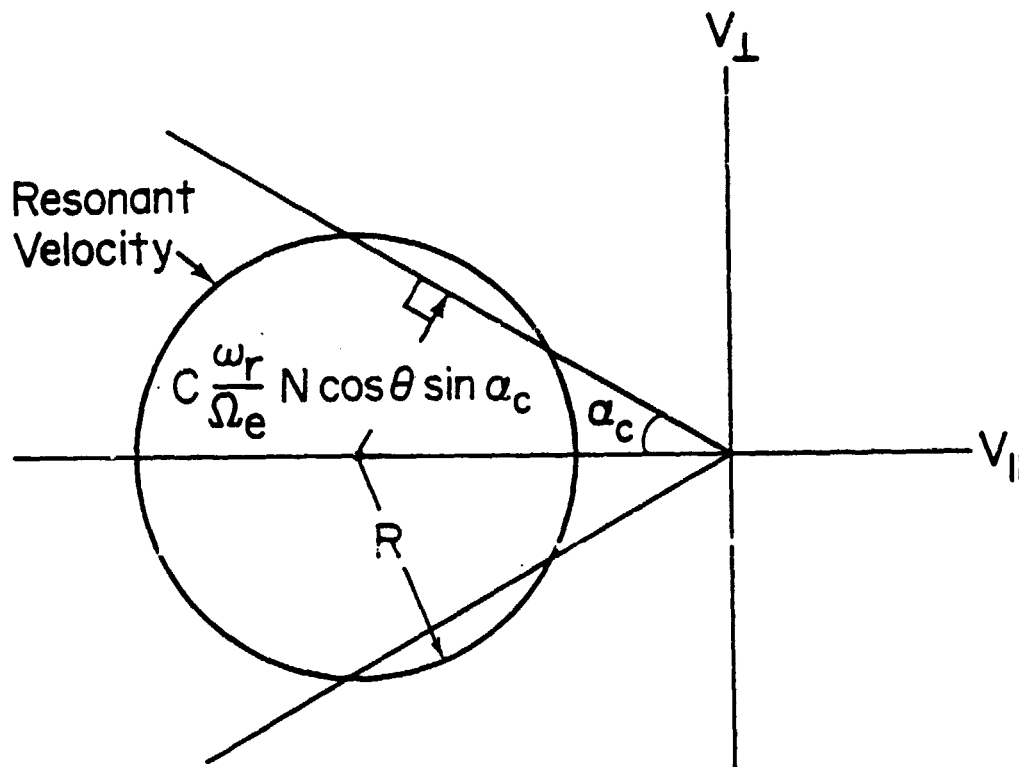
Case C is presented in Fig. 11. The upper panel displays the growth rate and the lower panel shows the real frequency. The abscissa in  $kc/\Omega_e$ . An interesting feature is that in this case the cutoff frequency becomes lower than the cyclotron frequency. Thus, even if  $k_{\parallel} = 0$ , wave-electron resonance is still possible. In fact, in this case, the growth rate is higher for  $\theta = 90^\circ$ . Except in the region  $kc \ll \Omega_e$ , the growth rate decreases rapidly as  $\theta$  decreases from  $90^\circ$ .

Lastly, we present case D in Fig. 12. In this case we find that the growth rate is significant only for  $0 \leq \theta \leq 45^\circ$ . For  $\theta > 45^\circ$ , the growth rate decreases rapidly. The growth rate  $\omega_i$  is computed for three values of  $\theta$ , namely  $\theta = 0^\circ$ ,  $\theta = 30^\circ$ , and  $\theta = 45^\circ$ . The result is about one order of magnitude smaller than that for case C. Furthermore, the bandwidth of the unstable mode for each given  $\theta$  is fairly narrow.

### C. Discussion

If we consider a loss-cone  $\alpha_c$  as indicated in Fig. 13 in which the boundary of the distribution function is shown to intersect with the resonance circle, the necessary condition for this to occur in that

ORIGINAL PAGE 13  
OF POOR QUALITY



$\alpha_c = \text{loss-cone angle}$

Fig. 13. Schematic Figure Depicting the Physics of the Amplification Process. The resonance surface is shown in typical dimension with respect to the upcoming atmospheric loss cone. Under normal circumstances the loss cone region will have negative anisotropy and contribute to wave growth.

$$c \frac{\omega_r}{\Omega_e} N \cos \theta \sin \alpha_c < R = c \sqrt{\frac{\omega_r^2}{\Omega_e^2} N^2 \cos^2 \theta - 2 \frac{\Delta \omega}{\Omega_e}} \quad (22)$$

This condition may be rewritten as

$$\frac{k^2 c^2}{\Omega_e^2} > 2 \left( \frac{\omega_r}{\Omega_e} - 1 \right) \frac{1}{\cos^2 \theta \cos^2 \alpha_c}$$

If we fix  $\alpha_c$  and  $(\omega_r/\Omega_e - 1)$ , it is seen that as  $\theta$  increases from  $0^\circ$ , the threshold value of  $kc/\Omega_e$  for instability also tends to increase. This explains why the threshold unstable wavenumber tends to shift to higher values when  $\theta$  changes from  $0^\circ$  to larger values, as shown in Fig. 10 and Fig. 12. For case C, the wave frequency  $\omega_r$  may be lower than  $\Omega_e$ . We see from Eq. (22) that in this case the instability can occur, even if  $k = 0$ . This observation agrees with the numerical result shown in Fig. 11.

It is true in general, that growth rate diminishes when  $k$  becomes sufficiently large. This is expected because the larger the  $k$ , the higher the  $\omega_r - \Omega_e$  and, therefore, the fewer the resonant electrons. The frequency bands of the unstable modes are fairly narrow for all cases studied in this paper, mainly because the characteristic electron energies at various altitudes which have been considered in the analysis are low. If we have assumed high energies, the growth rates would be even higher and the band widths of the unstable modes would be broader too.

The effects of a parallel electric field on the amplification of AKR are clearly significant and important. The parallel electric field not only modifies the distribution function but also reduces the density of the low-energy electrons. Both effects tend to increase the growth

rate at a given altitude. However, from our numerical studies, we find that the latter effect (density depletion) prevails over the former. However, some time when electron density is fixed, the two distribution functions (i. e., one with  $\Phi = 0$  and the other with  $\Phi \neq 0$ ) can give rise to significantly different growth rates. For instance, we have studied density model D3 and calculated the growth rates for the two cases. The difference between the dispersion relations is rather significant. As a result, the growth rates have quite different  $k$  dependence.

The present investigation also finds that the real loss-cone distribution function is more unstable (i. e., results in higher growth rates) than the effective loss-cone distribution function used by Lee et al., (1980). A comparative study is discussed by Wong et al., (1981) in which we examine the two cases in detail. The effective loss-cone distribution described by Eq. (1) peaks in  $v_{\perp}$  space about  $v_{\perp} \sim \alpha$  for whatever value of  $v_{\parallel}$ , whereas the real loss-cone distribution described by Eq. (2) peaks in  $v_{\perp}$  space at  $v_{\parallel} \tan \alpha_c$ . Thus the populations of resonant electrons for the two cases may be significantly different, if we fix the frequency  $\omega_{\perp}$ , and the wavevector  $k$ . Consequently, the growth rates obtained are not alike.

The major conclusions derived from the present study may be summarized as follows:

1.) The real loss-cone distribution function does give growth rates higher than that based on the effective loss-cone distribution.

2.) Within the context of the physical model and parameter regime which have been chosen for the numerical computation, we find that when  $n_b > n_e$  the growth rates are fairly uniform for waves propagating within a certain cone, say  $0 \leq \theta \leq \theta_0$ , where  $\theta$  is the angle between the

ambient magnetic field,  $\underline{B}$ , and the wavevector,  $\underline{k}$ . For case A or case B,  $\theta_0$  is about  $60^\circ$  and for case D ( $E_{\parallel} = 0$ )  $\theta_0$  is about  $45^\circ$ . On the other hand, if  $n_b = 0$ , the growth rate is highest when  $\theta \approx 90^\circ$ . The growth rate diminishes rapidly as  $\theta$  decreases.

3.) The spatial e-folding amplification distance is found typically of several tens of kilometers at  $4 \times 10^3$  km altitude and increases to a few hundred kilometers at  $8 \times 10^3$  km altitude for case A and B. For case D (no parallel electric field) the amplification distance increases rapidly with increasing altitude.

4.) If all low-energy electrons are assumed to be removed, the amplification can be very effective when a parallel electric field is present. We find in case C, the e-folding amplification distance at  $7 \times 10^3$  km altitude is less than a kilometer. This happens mainly because the local group velocity is very small.

5.) We have examined case C, but considered the distribution function with  $\Phi = 0$ . In this case we find that the cutoff frequency increases to a value very close to the cyclotron frequency and the growth rate decreases significantly from that we have obtained for case C. This implies that the effect of the parallel field on the unperturbed distribution is very important when the density of the low-energy background electrons is very low.

## BIBLIOGRAPHY

- Benson, R. F. and W. Calvert, ISIS-1 observations at the source of auroral kilometric radiation, *Geophys. Res. Lett.* 6, 479, 1979.
- Benson, R. F., W. Calvert, and D. M. Klumpar, Simultaneous wave and particle observations in the auroral kilometric source region, *Geophys. Res. Lett.*, 7, 959, 1980.
- Calvert, W., The auroral plasma cavity, University of Iowa, Department of Physics and Astronomy, Report, 81-9, May, 1981.
- Chiu, Y. T. and M. Schulz, Self consistent particle and parallel electrostatic field distributions in the magnetospheric ionospheric auroral region, *J. Geophys. Res.*, 83, 629, 1978.
- Croley, D. R., P. F. Mizera and J. F. Fennell, Signature of a parallel electric field in ion and electron distributions in velocity space, *J. Geophys. Res.*, 83, 2701, 1978.
- Fennell, J. F. and D. J. Gorney, Auroral particle distribution functions and their relationship to inverted-V's and auroral arcs, Proceedings of the Chapman Conference on the Formation of Auroral Arcs, 21-25 July 1980, Fairbanks, Alaska.
- Fried, B. D. and S. D. Conte, The Plasma Dispersion Function (Academic Press, Inc. New York, 1961).
- Grabbe, C. L., P. L. Palmadesso, and K. Papadopoulos, A coherent non-linear theory of auroral kilometric radiation, 1. Steady state model, *J. Geophys. Res.* 85, 3337, 1980.
- Gurnett, D. A. in Critical Problems of Magnetospheric Physics, ed. E. R. Dyer (National Academy of Sciences), p. 123.
- Gurnett, D. A. and J. Green, On the polarization and origin of auroral kilometric radiation, *J. Geophys. Res.* 83, 689, 1978.



- Kaiser, M. L., J. K. Alexander, A. C. Riddle, J. B. Pearce, and J. W. Warwick, Direct measurement by Voyagers 1 and 2 of the polarization of terrestrial kilometric radiation, *Geophys. Res. Lett.* 5, 857, 1978
- Kan, J. R., L. C. Lee, and S. I. Akasofu, Two dimensional potential double layer and discrete auroras, *J. Geophys. Res.* 84, 4305, 1979.
- Lee, L. C., J. R. Kan, and C. S. Wu, Generation of auroral kilometric radiation region, *Planet. and Space Sci.*, 28, 703, 1980.
- Melrose, D. B., An interpretation of Jupiter's decametric radiation and the terrestrial kilometric radiation as direct amplified gyroemission. *Astrophys. J.* 207, 651, 1976.
- Mizera, P. F. and J. F. Fennell, Signatures of electric fields from high and low altitude particle distributions, *Geophys. Res. Lett.*, 4, 311, 1977.
- Mozer, F. S., C. W. Carlson, M. K. Hudson, R. B. Torbert, B. Parady, J. Yatteau, and M. C. Kelley, Observations of paired electrostatic shocks in the polar magnetosphere, *Phys. Rev. Lett.*, 83, 292, 1974.
- Shawhan, S., C. G. Falthammer and L. P. Block, On the Nature of Large Auroral Zone Electric Fields at  $1-R_E$  Altitude, *J. Geophys. Res.* 83, 1049, 1978.
- Shkarofsky, I. P., Dielectric Tensor in Vlasov Plasmas near Cyclotron Harmonics, *Phys. Fluids* 9, 561, 1966.
- Tsai, S. T., C. S. Wu, Y. D. Wang and S. W. Kang, Dielectric tensor of a weakly relativistic, nonequilibrium and magnetized plasma. (To be published in *Phys. Fluids*, 1981.)
- Wescott, E. M., H. C. Stenback-Nielsen, T. J. Halliman, T. N. Davis and H. M. Peek, The Skylab Barium Plasma Injection Experiments, 2. Evidence for a Double Layer, *J. Geophys. Res.* 81, 4495, 1976.
- Wu, C. S. and L. C. Lee, A theory of the terrestrial kilometric radiation, *Astrophys. J.* 230, 621, 1979.

Wu, C. S., The source mechanism of auroral kilometric radiation, In the Proceedings of the Formation of Auroral Arcs, July 21-25, 1980.

APPENDIX

The Functions of  $\phi_j$ ,  $g_\alpha$ , and  $f_\beta$

After some straightforward algebra, one can show that

$$\phi_1 \equiv -\frac{1}{b} \left( \frac{\phi}{\alpha^2} - \frac{\phi}{\alpha^2} \frac{k_{||}\alpha}{\omega} h + \frac{h^2}{\mu^2} - \frac{k_{||}\alpha}{\omega} \frac{h^3}{\mu^2} \right)$$

$$\phi_2 = \frac{1}{b} \left( \frac{\phi}{\alpha^2} + \frac{h^2}{\mu^2} \right) - \frac{1}{b} \left( \frac{\phi}{\alpha^2} \frac{k_{||}\alpha}{\omega} h + \frac{1}{2\mu} - \frac{2h^2}{\mu^2} - \frac{3}{2} \frac{k_{||}\alpha}{\omega} \frac{h}{\mu} + \frac{3k_{||}\alpha}{\omega} \frac{h^3}{\mu^2} \right)$$

$$\phi_3 \equiv \left( 1 + \frac{1}{2\mu b} - \frac{2h^2}{b\mu^2} \right) - \frac{1}{b} \left( \frac{h^2}{\mu^2} + \frac{3}{2} \frac{k_{||}\alpha}{\omega} \frac{h}{\mu^2} - \frac{3k_{||}\alpha}{\omega} \frac{h^3}{\mu^2} \right)$$

$$\phi_4 \equiv \frac{h^2}{b\mu^2} - \frac{1}{b} \frac{k_{||}\alpha}{\omega} \frac{h^3}{\mu^2}$$

$$g_1 = -\frac{1}{b} \left( \frac{\phi}{\alpha^2} \frac{h}{\mu} - \frac{\phi}{\alpha^2} \frac{k_{||}\alpha}{\omega} \frac{h^2}{\mu} + \frac{h^3}{\mu^3} - \frac{k_{||}\alpha}{\omega} \frac{h^4}{\mu^3} \right)$$

$$g_2 \equiv \frac{2\phi}{\alpha^2 b} \frac{h}{\mu} + \frac{4h^3}{b\mu^3} + \frac{1}{2} \frac{\phi}{\alpha^2} \frac{1}{b} \frac{k_{||}\alpha}{\omega} - \frac{\phi}{\alpha^2} \frac{k_{||}\alpha}{\omega} \frac{h^2}{b\mu} - \frac{3h}{2b\mu^2} + \frac{k_{||}\alpha}{\omega} \frac{3h^2}{\mu^2} - \frac{k_{||}\alpha}{\omega} \frac{4h^4}{b\mu^3}$$

$$g_3 \equiv -\frac{\phi}{\alpha^2 b} \frac{h}{\mu} + \frac{h}{\mu} + \frac{3h}{b\mu^2} - \frac{6h^3}{b\mu^3} + \frac{\phi}{\alpha^2} \frac{k_{||}\alpha}{\omega} \frac{h^2}{b\mu} + \frac{3}{4} \frac{k_{||}\alpha}{\omega} \frac{1}{b\mu} - 6 \frac{k_{||}\alpha}{\omega} \frac{h^2}{b\mu^2} + 6 \frac{k_{||}\alpha}{\omega} \frac{h^4}{b\mu^3}$$

$$g_4 \equiv \frac{h}{\mu} - \frac{3}{2} \frac{h}{b\mu^2} + \frac{4h^3}{b\mu^3} + \frac{k_{||}\alpha}{b\omega} \frac{3h^2}{\mu^2} - \frac{k_{||}\alpha}{\omega} \frac{4h^4}{b\mu^3}$$

$$g_5 \equiv -\frac{h^3}{b\mu^3} + \frac{k_{||}\alpha}{\omega} \frac{h^4}{b\mu^3}$$

$$f_1 \equiv \left( -\frac{\phi}{\alpha^2} \frac{h}{b\mu} + \frac{\phi}{\alpha^2} \frac{k_{11}\alpha}{\omega} \frac{h^2}{b\mu} - \frac{h^3}{b\mu^3} + \frac{k_{11}\alpha}{\omega} \frac{h^4}{b\mu^3} \right) \frac{h}{\mu}$$

$$f_2 \equiv \frac{3\phi}{\alpha^2} \frac{h^2}{b\mu^2} + \frac{5h^4}{b\mu^4} - \frac{\phi}{\alpha^2} \frac{1}{2b\mu} + \frac{\phi}{\alpha^2} \frac{k_{11}\alpha}{\omega} \frac{3h}{2\mu b}$$

$$- \frac{\phi}{\alpha^2} \frac{k_{11}\alpha}{\omega} \frac{3h^3}{b\mu^2} - \frac{3h^2}{b\mu^3} + \frac{k_{11}\alpha}{\omega} \frac{5h^3}{b\mu^3} - \frac{k_{11}\alpha}{\omega} \frac{5h^5}{b\mu^5}$$

$$f_3 \equiv \frac{\phi}{2\alpha^2 b\mu} - \frac{\phi}{\alpha^2} \frac{3h^2}{b\mu^2} + \frac{9h^2}{b\mu^3} + \frac{h^2}{\mu^2} - \frac{10h^4}{b\mu^4} - \frac{\phi}{\alpha^2} \frac{k_{11}\alpha}{\omega} \frac{3h}{2b\mu}$$

$$+ \frac{\phi}{\alpha^2} \frac{k_{11}\alpha}{\omega} \frac{3h^3}{b\mu^2} - \frac{3}{4b\mu^2} + \frac{k_{11}\alpha}{4\omega} \frac{15h}{b\mu^2} - \frac{k_{11}\alpha}{\omega} \frac{15h^3}{b\mu^3} + \frac{k_{11}\alpha}{\omega} \frac{10h^5}{b\mu^4}$$

$$f_4 \equiv \frac{\phi}{\alpha^2} \frac{h^2}{b\mu^2} + \frac{1}{2\mu} - \frac{2h^2}{\mu^2} + \frac{3}{4b\mu^2} - \frac{9h^2}{b\mu^3} + \frac{10h^4}{b\mu^4} - \frac{\phi}{\alpha^2} \frac{k_{11}\alpha}{\omega} \frac{h^3}{b\mu^2}$$

$$- \frac{k_{11}\alpha}{\omega} \frac{15h}{4b\mu^2} + \frac{k_{11}\alpha}{\omega} \frac{15h^3}{b\mu^3} - \frac{k_{11}\alpha}{\omega} \frac{10h^5}{b\mu^4}$$

$$f_5 \equiv \frac{h^2}{\mu^2} + \frac{3h^2}{b\mu^3} - \frac{5h^4}{b\mu^4} - \frac{5k_{11}\alpha h^3}{\omega b\mu^3} + \frac{k_{11}\alpha}{\omega} \frac{5h^3}{b\mu^4}$$

and

$$f_6 \equiv \frac{h^4}{b\mu^4} - \frac{k_{11}\alpha}{\omega} \frac{h^5}{b\mu^4}$$